The Astrophysical Journal, 776:113 (20pp), 2013 October 20 doi:10.1088/0004-637X/776/2/113

SPECTROPOLARIMETRY OF THE CLASSICAL T TAURI STAR BP TAU

Wei Chen and Christopher M. Johns-Krull
Department of Physics & Astronomy, Rice University, Houston, TX 77005, USA; wc2@rice.edu, cmj@rice.edu
Received 2011 August 15; accepted 2013 August 21; published 2013 October 4

ABSTRACT

We implement a least-squares deconvolution (LSD) code to study magnetic fields on cool stars. We first apply our code to high-resolution optical echelle spectra of 53 Cam (a magnetic Ap star) and three well-studied cool stars (Arcturus, 61 Cyg A, and ξ Boo A) as well as the Sun (by observing the asteroid Vesta) as tests of the code and the instrumentation. Our analysis is based on several hundred photospheric lines spanning the wavelength range 5000 Å to 9000 Å. We then apply our LSD code to six nights of data on the Classical T Tauri Star BP Tau. A maximum longitudinal field of 370 ± 80 G is detected from the photospheric lines on BP Tau. A 1.8 kG dipole tilted at 129° with respect to the rotation axis and a 1.4 kG octupole tilted at 104° with respect to the rotation axis, both with a filling factor of 0.25, best fit our LSD Stokes *V* profiles. Measurements of several emission lines (He I 5876 Å, Ca II 8498 Å, and 8542 Å) show the presence of strong magnetic fields in the line formation regions of these lines, which are believed to be the base of the accretion footpoints. The field strength measured from these lines shows night-to-night variability consistent with rotation of the star.

Key words: stars: formation – stars: individual (BP Tau) – stars: magnetic field – stars: pre-main sequence – techniques: polarimetric

Online-only material: color figures

1. INTRODUCTION

T Tauri Stars (TTSs) are young low-mass pre-main-sequence stars at a typical age of a few million years. BP Tau is a Classical T Tauri Star (CTTS). Originally defined by their Hα equivalent width, CTTSs are found to still be accreting material from their circumstellar disks, whose existence is usually inferred by an infrared (IR) continuum excess. The most popular model describing the interaction of a CTTS with its disk is the so-called "magnetospheric accretion" model (e.g., Camenzind 1990; Hartmann et al. 1994; Shu et al. 1994), which posits that strong stellar magnetic fields truncate the inner disk at a point near the corotation radius. Material from the disk attaches to the field lines and flows onto the central star, creating accretion shocks at the surface. Magnetic fields are also thought to provide braking torques that prevent the stellar rotation from increasing to near the breakup velocity as a result of the angular momentum the star gains from the accreting material. This is invoked to explain why observed rotation velocities are usually an order of magnitude smaller than the breakup velocity (e.g., Hartmann & Stauffer 1989). Therefore, measuring the magnetic fields on CTTSs and probing the field geometry are of great importance in understanding the general picture of how a CTTS interacts with its surrounding disk and maintains its relatively slow rotation rate.

The Zeeman effect is widely used to detect and measure magnetic fields. In the presence of a magnetic field, a single degenerate energy level of the electrons in atoms and molecules can be split into several sublevels. Thus, a spectral line corresponding to a transition between two degenerate levels can be split into several different components. Some components are linearly polarized, called the π components, while the others are either left or right elliptically polarized, called the σ components (left as σ^+ and right as σ^-). The relative strength of these components depends on the viewing angle relative to the direction of the magnetic field. If the line of sight is parallel to the direction of the magnetic field, the π components vanish and the σ components are circularly polarized. Otherwise, all of the components are present. After passing through a left-handed circular analyzer, a majority portion of each σ^+ component, half of each π component, and a smaller portion of each σ^- component are present in the left circularly polarized spectrum (*L*); while a majority portion of each σ^- component, half of each π component, and a smaller portion of each σ^+ component are able to pass through a right-handed circular analyzer, making up the corresponding line in the right circularly polarized spectrum (*R*). The Stokes *I* and *V* spectra can be obtained by adding and subtracting the continuum normalized *R* and *L*,

$$I = \frac{R+L}{2}, V = \frac{R-L}{2}, \quad (1)$$

where *I* is the total unpolarized spectrum while *V*, the circularly polarized portion, potentially contains Zeeman signatures for all of the lines present in the spectrum. Generally, the total magnetic field, *B*, can be measured from Stokes *I* while both circularly polarized spectra *R* and *L* or both Stokes *I* and *V* are needed to obtain the longitudinal (or line of sight) field, B_z.

For resolved splitting when the fields are strong enough, measuring the shifts of σ^+ and σ^- components with respect to the nominal wavelength in Stokes *I* gives *B* directly. For a component corresponding to a transition from level 2 to level 1,

$$\Delta\lambda = \lambda - \lambda_0 \approx -(m_2 g_2 - m_1 g_1)\frac{e}{4\pi m_e c^2}{\lambda_0}^2 B = -4.67 \times 10^{-13}(m_2 g_2 - m_1 g_1){\lambda_0}^2 B, \quad (2)$$

where *m* is the quantum number for J_z, *g* is the Landé-*g* factor for the level, and *B* is the magnetic field strength. The relative intensities of different components in *R* and *L* are indicators of the field orientation with respect to the line of sight, which can then be used to determine B_z. On the other hand, for unresolved splitting, different components are blended, which can result in the broadening of the corresponding spectral line in Stokes *I*.

Measuring this broadening can also give the total magnetic field. If the unpolarized beam passes through a right or left-handed circular analyzer, the spectrum present in either R or L is a single broadened line for the transition with no clear splitting; however, there can be a slight shift of the line in the R or L spectrum due to the different weighting of the unresolved π and σ components. Then, B_z can be obtained by calculating the shift between the line observed in R and L light (λ_r and λ_l respectively),

$$\Delta\lambda = \lambda_r - \lambda_l = 2 \times \frac{e}{4\pi m_e c^2} \lambda^2 g_{\rm eff} B_z = 9.34 \times 10^{-13} \lambda^2 g_{\rm eff} B_z, \quad (3)$$

where λ is the nominal wavelength for this line and $g_{\rm eff}$ is the effective Landé-g factor for this atomic transition and is determined by an intensity weighted mean for all of the σ subcomponents that make up the line.

Generally, for late type stars whose magnetic fields are believed to be weak, measuring Zeeman broadening from several magnetically sensitive spectral lines in unpolarized Stokes I spectra is the best choice to get the total magnetic field strength (Mathys 1991; Valenti et al. 1995; Johns-Krull & Valenti 1996). However, in CTTSs, because of the generally more rapid rotation, Zeeman broadening is usually masked by Doppler broadening, which makes detection of magnetic broadening in optical spectra more difficult. This is why Basri et al. (1992) instead made use of optical absorption lines near or on the flat part of the curve of growth to measure the enhancement of the equivalent widths due to the shifts of the Zeeman components to determine the mean field strength. They detected excess equivalent width in lines from spectra of the Naked T Tauri Star (NTTS) Tap 35 which they interpreted as evidence for a field of about 1000 G covering the entire surface, or for stronger fields covering a smaller portion of the surface, but with an upper limit of about 1500 G on the field strength. Despite the difficulty in applying the Zeeman broadening method to CTTSs, Johns-Krull et al. (1999b) carefully determined stellar parameters ($v \sin i$, log g, $T_{\rm eff}$, $v_{\rm turb}$) of BP Tau and examined the strongly magnetically sensitive Ti I line at 2.2233 μm and measured a mean surface field of 2.6 $\pm$ 0.3 kG using Zeeman broadening. Yang et al. (2005) applied the same procedure to four magnetically sensitive Ti I lines near 2.2 μm from the spectra of TW Hydrae and obtained a mean field of 2.61 $\pm$ 0.23 kG. This technique has now been applied to many TTSs (Johns-Krull 2007; Yang et al. 2008; Yang & Johns-Krull 2011).

Spectropolarimetry is often used to measure the mean longitudinal magnetic field, B_z, by measuring shifts between the corresponding lines in right and left circularly polarized spectra (Mathys 1991; Johns-Krull et al. 1999a; Valenti & Johns-Krull 2004). Spectropolarimetric observations are generally sensitive to weaker fields than the Zeeman broadening technique; however, in the limit of no stellar rotation, polarimetry is only sensitive to the net field and suffers from cancellation of opposite field polarities. On rotating stars, the cancellation is not quite as severe, depending on the geometry of the field, and can produce signatures in Stokes V even when the net field is 0. In the case of a rotating star, time series observations of Stokes V can be used to probe the large-scale magnetic field geometry. One direct way to measure B_z is to calculate the shift between the right and left circularly polarized components (Equation (3)). This has routinely been applied to stars which have fields with strong line-of-sight field components, such as some Ap and Bp stars, which possess strong, globally organized fields and whose temporal variations can usually be interpreted by the oblique rotator model (Borra & Landstreet 1980). A good example is Babcock's Star (HD 215441), the nondegenerate star with the strongest magnetic field (34 kG) detected so far (Babcock 1960). For weak fields, the shift is not often resolved, i.e., the Zeeman signatures are weak, which is often the case for the photospheric lines of CTTSs. This can make it very difficult to detect Zeeman signatures or longitudinal fields by using single lines. Multiple-line techniques (e.g., least-squares deconvolution—LSD) have been developed to extract these weak signatures in Stokes V profiles by effectively averaging over hundreds to thousands of spectral lines (Donati et al. 1997; Donati et al. 2008). LSD is widely used to measure weak magnetic fields on different types of stars along the Hertzsprung–Russell diagram, such as Ap and Bp stars (Wade et al. 2000a), late type stars (Barnes 1999), and T Tauri Stars (Donati et al. 2007; Hussain et al. 2009), including BP Tau (Donati et al. 2008). It has the advantage of greatly enhancing the signal-to-noise ratio (S/N) of the obtained intrinsic Stokes I and V profiles, permitting a sensitive measurement of weak mean longitudinal magnetic fields. Here, we develop our own LSD code and apply it to six nights of observations of BP Tau. This paper is organized as follows. In Section 2 we describe our observations and data reduction procedures. In Section 3, we describe the LSD method, the center-of-gravity (COG) method, and the integral method for recovering mean field strengths, and present results for photospheric field measurements on our observed stars. In Section 4, results on the three emission lines of BP Tau are given. In Section 5, we discuss our results, and Section 6 presents a summary.

2. OBSERVATIONS AND DATA REDUCTION

All data were obtained at the 2.7 m Harlan J. Smith Telescope at McDonald Observatory using the Zeeman analyzer (ZA) and cross-dispersed coudé echelle spectrometer (2dcoudé; Tull et al. 1995). The ZA system was developed by Vogt et al. (1980) and originally used to search for fields on cool main sequence stars. The basic ZA system remains the same, but its usage now with 2dcoudé has been described in detail by Johns-Krull et al. (1999a), Daou et al. (2006), and Yang et al. (2007), where it was shown that the ZA system delivers polarization measurements in excellent agreement with previous results. Here, we only summarize the basics of how circular polarization observations are made. The incoming light beam, first corrected by a Babinet–Soleil phase compensator to reduce the spurious linear polarization produced by the flat bounces in the coudé mirror train, goes through the ZA and is split into two beams, a left circularly polarized component and a right circularly polarized one. The two parallel beams enter the spectrometer slit. Two copies of the spectrum are recorded on a 2080 $\times$ 2048 CCD with a two-pixel resolution of $R = \lambda/\Delta\lambda \approx 60{,}000$. For each night, one or two pairs of exposures were taken for each target. Between each exposure, an achromatic 1/2 wave plate was used to reverse the sense of circular polarization of the two beams. The purpose of taking pairs of exposures for each object is to cancel out potential systematic effects such as the possible existence of spatial shifts on the detector due to any tilt between the slit and the CCD. Additionally, taking two pairs of exposures (four total exposures) provides a null check on our instrumentation and methods (see Section 3.5.3 for details). Using a pair of exposures introduces the possibility of a temporal drift in the wavelength scale from one exposure to the next; however, averaging only two observations cancels out such a drift to first order and still provides useful polarization measurements (e.g., Donati et al. 1997). From UT date 1998 November 26 to 1998 December 1 we observed BP Tau and

Table 1
Observations

Star	UT Date	UT Time	Julian Date (2400000+)	N_{exp}	Expo Time (s)	S/N	$Noise_{LSD}$ ($\times 10^{-4}$ I_c)
Sun	1997 Nov 24	03:28	50776.644	2	900	300	2.7
Arcturus	1998 Dec 1	12:42	51179.029	2	10	700	2.4
61 Cyg A	1999 Apr 20	11:31	51288.980	4	1100	1000	1.8
	1999 Apr 25	11:31	51293.980	4	1320	900	1.7
	1999 Apr 26	11:39	51294.985	2	940	600	2.2
61 Cyg B	1999 Nov 25	02:25	51507.601	2	900	250	...
ξ Boo A	1999 Apr 20	07:50	51288.826	4	800	1000	1.9
	1999 Apr 21	10:17	51289.928	4	860	1000	1.4
	1999 Apr 22	11:17	51290.970	4	1030	1000	1.5
	1999 Apr 23	10:13	51291.926	4	1450	1200	1.3
	1999 Apr 25	03:52	51293.661	4	3000	1200	1.1
	1999 Apr 26	10:23	51294.933	4	2600	1200	0.97
BP Tau	1998 Nov 26	05:19	51143.722	2	3600	50	27
	1998 Nov 27	03:05	51144.628	2	6700	60	30
	1998 Nov 28	03:21	51145.647	2	6000	60	20
	1998 Nov 29	03:15	51146.635	2	6000	50	34
	1998 Nov 30	04:05	51147.670	2	6000	40	33
	1998 Dec 1	03:27	51148.644	2	5000	70	20

Babcock's Star each night; from 1999 April 20 to 1999 April 26, ξ Boo A and 53 Cam were observed. Details of these observations including observing dates and times, number of exposures, S/N per pixel, and noise level are given in Table 1. We used the echelle reduction package described in Valenti (1994) to reduce all the spectra, and the spectra of a thorium-argon lamp was used to determine the wavelength solution.

Part of the analysis presented below also utilizes a higher spectral resolution observation of the K7V star 61 Cyg B, also obtained with 2dcoudé on the 2.7 m telescope. For this observation, the CCD was placed at the F1 focus of the instrument where a 0.″59 slit yielded a spectrum with a resolution of $R = 121{,}000$ with 4.65 pixels per resolution element. The ZA system was not in place while 61 Cyg B was observed at this higher resolution. This observation also appears in Table 1; however, only Stokes I was recorded on this date (1998 November 25). The data reduction, including the wavelength calibration, was performed in the same manner as described above for the lower resolution spectra. The analysis of this data concentrates on the magnetically sensitive Fe I line at 8468.40 Å. The final spectrum in this region has a continuum S/N of ~250 for this spectrum of 61 Cyg B.

3. LEAST-SQUARES DECONVOLUTION AND PHOTOSPHERIC LINES

3.1. Least-squares Deconvolution

The LSD method makes several assumptions: (1) all spectral lines have essentially the same intrinsic shape; (2) the local intensity of each line is proportional to line central depth, d, that is, the lines are all on the linear portion of the curve of growth; (3) depths of blended lines add up linearly; (4) limb darkening is independent of wavelength; and (5) the lines satisfy the weak field approximation. Assumptions (1), (2), and (3) are not applicable to optically thick lines but are reasonably good approximations for relatively optically thin lines. Assumption (4) guarantees that line ratios between any two lines remain the same after integration of the intensity over the whole star. Assumption (5) yields that the weight for Stokes V spectrum for each line is proportional to the product of the line wavelength, the mean Landé-g factor, and the line central depth.

We follow the same procedures as described in Donati et al. (1997). Note that the spectra used here have already been normalized to unit continuum. According to the assumptions above, for a single line,

$$Y(v) = wZ(v) \tag{4}$$

where Y is the local Stokes I ($1 - I$ in practice) or V spectrum, w is the weight for this line, and Z is the intrinsic Stokes I or V profile with the instrumental broadening included and is the same for all of the lines. The weight, w, is d for $(1 - I)$ and $g\lambda d$ for V, where λ is the line wavelength, g is the mean Landé-g factor, and d is the line central depth. For the actual spectrum containing thousands of lines, the Stokes I or V spectrum is the convolution of the sum of thousands of delta functions with the intrinsic Stokes I or V profile:

$$Y(v) = \int Z(v - v')M(v')\,dv', \tag{5}$$

where $M(v) = \sum_i w_i \delta(v - v_i)$. Therefore,

$$Y(v) = \sum_i w_i Z(v - v_i), \tag{6}$$

i.e., $\mathbf{Y} = \mathbf{M} \cdot \mathbf{Z}$ in matrix format, where $\mathbf{Z}$ is a vector to be determined, $\mathbf{M}$ is the 2-D weight matrix weighted by λgd when calculating Stokes V, while the weights are just d for Stokes I, and $\mathbf{Y}$ is a vector of the Stokes I $(1 - I)$ or V spectrum. Using linear LSD, the solution for this gives the intrinsic Stokes profile as:

$$\mathbf{Z} = (\mathbf{M}^t \cdot \mathbf{S}^2 \cdot \mathbf{M})^{-1}(\mathbf{M}^t \cdot \mathbf{S}^2 \cdot \mathbf{Y}). \tag{7}$$

The matrix $\mathbf{S}$ is diagonal and its elements are the reciprocals of the uncertainties for the elements of $\mathbf{Y}$. The diagonal elements of $(\mathbf{M}^t \cdot \mathbf{S}^2 \cdot \mathbf{M})^{-1}$ are the variance of the resultant vector $\mathbf{Z}$. Hence, the average Stokes I and V spectra will be

$$I = 1 - \bar{d}Z_I \quad V = \bar{\lambda}\bar{g}\bar{d}Z_V \tag{8}$$

where a bar on the top indicates taking average values over the line list used in the LSD method. The vector Z_I is the intrinsic Stokes I profile and the vector Z_V is the intrinsic Stokes V profile calculated in Equation (7).

As described below, we primarily base our signal detection on the significance of our B_z measurements. In addition, to help quantify the significance of signal detection, we use the false alarm probability (FAP) suggested by Donati et al. (1992) and the same convention as used by Donati et al. (1997) and Kochukhov et al. (2011): an FAP of less than 10^{-5} suggests a definite detection, an FAP of from 10^{-5} to 10^{-3} suggests a marginal detection, and an FAP of larger than 10^{-3} suggests a null detection.

3.2. Line Selection

The first step in using the LSD method is to create a line list containing the wavelength, the mean Landé g factors, and the central depths of the lines to be used. We use the Vienna Atomic Line Database (VALD; Kupka et al. 1999) and pick lines in the following manner: predicted line depths are greater than 0.2. Lines should not be in regions where strong lines (such as Balmer and Ca II H & K and Na I D lines) or telluric lines appear. Spectral lines of rotating stars such as BP Tau are rotationally broadened first before picking lines with $d > 0.2$. VALD does not have an option to include rotation when estimating the central depth. Therefore, we run the SYNTHMAG (Piskunov 1999) line synthesis code on each line and rotationally broaden them and find the theoretical central depth for each broadened line. Since the weakest lines with $d < 0.2$ do not contribute much to the spectrum and have lower S/N compared to stronger lines, including them primarily consumes more computer time and can actually increase the noise in the resultant LSD profile. The handling of the uncertainties is described in Section 3.4.

3.3. Center-of-gravity Method and Integral Method

The COG method (Mathys & Lanz 1992) calculates the average line center wavelength, or velocity, weighted by the local line depth across a proper wavelength or velocity range:

$$x_{\rm cog} = \frac{\int x[1 - I(x)]\,dx}{\int [1 - I(x)]\,dx}, \tag{9}$$

where x can be λ or v, and I can be replaced by R or L to get the COG in either the right or left circularly polarized spectrum. We can construct LSD right and left circular polarized spectra by adding and subtracting the average LSD Stokes I and V spectra,

$$R = I + V,\ L = I - V. \tag{10}$$

From the right and left circular polarized spectra R and L, we can then use the COG method to calculate the line center wavelengths, λ_r and λ_l, or velocities, v_r and v_l, and then use the following to calculate the mean longitudinal field B_z:

$$\Delta\lambda = \lambda_r - \lambda_l = 2 \times \frac{e}{4\pi m_e c^2}\bar{\lambda}^2\bar{g}B_z = 9.34 \times 10^{-13}\bar{\lambda}^2\bar{g}B_z, \tag{11}$$

or

$$\Delta v = v_r - v_l = 2 \times \frac{e}{4\pi m_e c}\bar{\lambda}\bar{g}B_z = 2.80 \times 10^{-7}\bar{\lambda}\bar{g}B_z, \tag{12}$$

where wavelengths, λ, are in Å, velocities, v, are in km s^{-1}, and the field, B_z, is in G.

The so-called integral method is equivalent to the COG method as long as $\int [1 - R(x)]\,dx = \int [1 - L(x)]\,dx = \int [1 - I(x)]\,dx$, which is valid when the assumptions (1), (2), (3), and (5) hold (Mathys 1989). Then

$$B_z = -\frac{4\pi m_e c^2}{e\bar{\lambda}^2\bar{g}}\frac{\int \lambda V(\lambda)\,d\lambda}{\int [1 - I(\lambda)]\,d\lambda} = -\frac{2.14 \times 10^{12}}{\bar{\lambda}^2\bar{g}}\frac{\int \lambda V(\lambda)\,d\lambda}{\int [1 - I(\lambda)]\,d\lambda}, \tag{13}$$

or

$$B_z = -\frac{4\pi m_e c}{e\bar{\lambda}\bar{g}}\frac{\int vV(v)\,dv}{\int [1 - I(v)]\,dv} = -\frac{7.14 \times 10^{6}}{\bar{\lambda}\bar{g}}\frac{\int vV(v)\,dv}{\int [1 - I(v)]\,dv}, \tag{14}$$

where wavelengths, λ, are in Å, velocities, v, are in km s^{-1}, and the field, B_z, is again in G. In practice, we calculate B_z in discrete velocity space. Assuming the bounds of the integration are pixel m (lower bound) and pixel n (upper bound), we then have the integral method in the form as follows:

$$B_z = -\frac{7.14 \times 10^{6}}{\bar{\lambda}\bar{g}}\frac{\sum_{i=m}^{n} v_i V_i}{\sum_{i=m}^{n}(1 - I_i)}, \tag{15}$$

$$\sigma_{B_z} = |B_z|\sqrt{\frac{\sum_{i=m}^{n} v_i^2\sigma_{Vi}^2}{|\sum_{i=m}^{n} v_i V_i|^2} + \frac{\sum_{i=m}^{n}\sigma_{Ii}^2}{|\sum_{i=m}^{n}(1 - I_i)|^2}}, \tag{16}$$

where σ_{B_z} is the uncertainty. Since the integral method and the COG method give nearly identical results, we do not discuss the COG method any further. The integral method is used in all of the cases for the rest of this paper.

3.4. Uncertainties

Uncertainties in the LSD Stokes I or V spectrum determined by propagating through the uncertainties in the original observed spectra returned by the reduction routine are much smaller than the standard deviation of the noise in the wings of the final LSD Stokes spectra where the signal is expected to be constant except for the noise. In addition, in the far wings (the continuum), the Stokes V spectra are expected to be zero while the Stokes I spectra should be unity. Explaining the extra apparent noise in the LSD profiles as a result of underestimating the uncertainties in the observed spectra is ruled out since the standard deviation of the observed continuum in the original spectra is comparable with the uncertainty estimated for each pixel. This indicates that there are additional sources of uncertainty present in the final LSD profile. First, an incomplete line list is used. Though modern atmosphere models are already very sophisticated and robust, they are not perfect, and the line lists used to create them inevitably contain errors. There are lines that are in the actual spectra but not in the line lists and vice versa. The lines we adopted have limits on their central depth, which exclude the weakest lines that have a chance of blending with the lines actually used. Second, though related, line lists from VALD and the spectrum synthesis from SYNTHMAG do not perfectly reproduce the line depths in the observed spectra. An implicit assumption in all LSD analysis is that these line list errors are averaged out by using several hundred to a few thousand lines. Third, many of the LSD assumptions made are not strictly valid. Intrinsic line profile shapes can differ from one line to another. Kochukhov et al. (2010) assessed the validity of the line self-similarity assumption and found a discrepancy between the line profiles from a detailed spectrum synthesis calculation. With a spectral resolution of 60,000, the

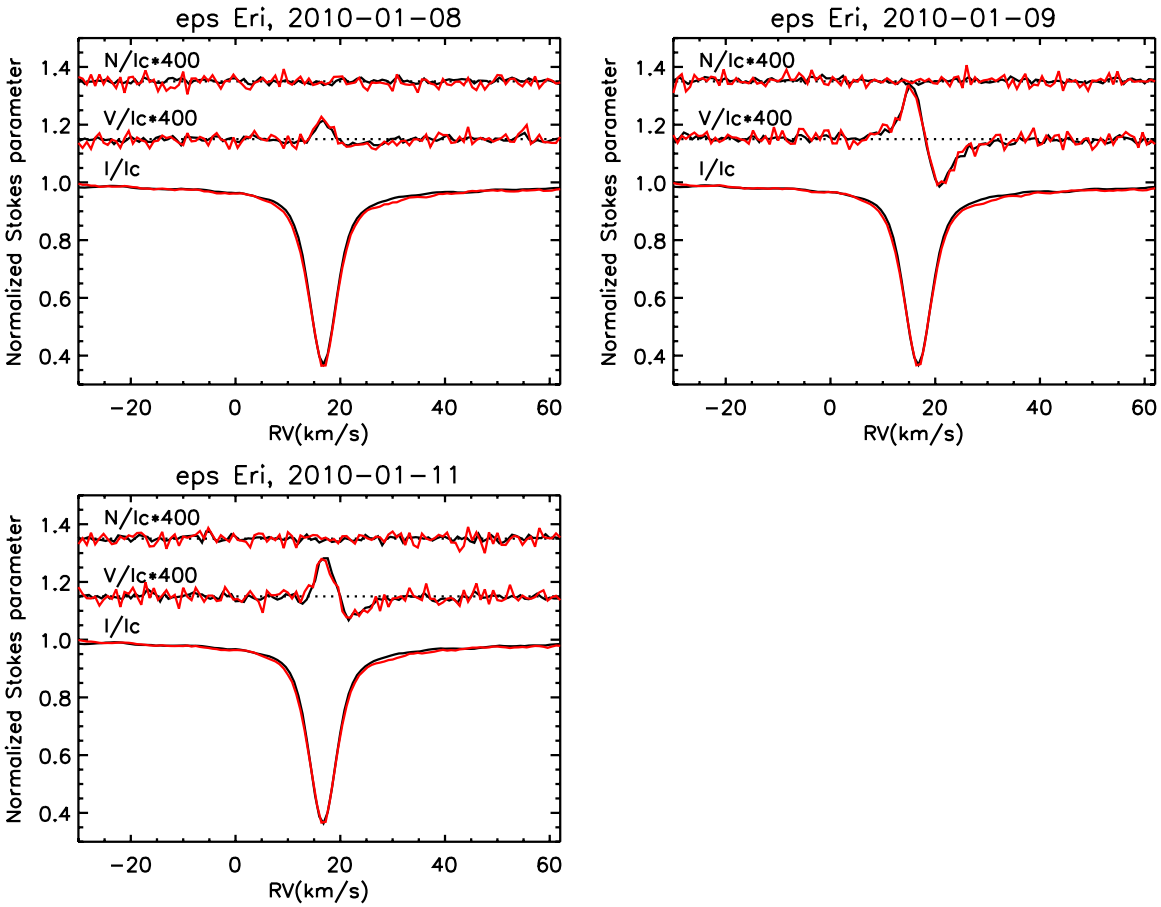

Figure 1. Comparison between the LSD Stokes *I* and *V* and null (N) profiles of ϵ Eri by Kochukhov et al. (2011; black) and this work (red) using the same data set and the same line list. The agreement between the two are quite good.

(A color version of this figure is available in the online journal.)

discrepancy is greater than 10% for the lines with central depths greater than 40%. Fourth, instrument resolution is not infinite. We are using a high-resolution instrument with a two-pixel resolution of $R = \lambda/\delta\lambda \approx 60{,}000$, about 5.0 km s^{-1} in velocity space. Finally, limb darkening can vary with wavelength. As a result of all of these potential sources of error, we elect to use the standard deviation of the noise in the final LSD Stokes spectra as the uncertainties appropriate for the Stokes profiles when determining the field strength. This enables us to include contributions to the uncertainty from the additional sources mentioned above.

3.5. Tests

For a polarization study such as the one we present here for BP Tau, there are three broad sources of potential systematic error. The first could result from some error in the analysis software, particularly the LSD code which is reasonably complex. The second could result from the instrumentation itself, possibly producing recorded spectra that do not accurately measure the level of polarization present. For a system such as the ZA used at the coudé focus of the McDonald 2.7 m telescope, the typical instrumental error is incomplete correction by the Babinet–Soleil phase compensator which results in a loss of efficiency in sensitivity to true circular polarization and an underestimate of the true signal (Vogt 1978; Vogt et al. 1980). A third potential source of error, also primarily instrumental in nature, can be caused by some unaccounted for shift in the spectra recorded in the two polarization states. Such a shift would produce a spurious measurement of polarization and inference of a magnetic field when none is present. This effect can be thought of as a zero-point error. We performed tests for each of these possibilities. We then turn to the analysis of our primary science target, BP Tau.

3.5.1. Test of the LSD Code

Kochukhov et al. (2011) present their spectropolarimetric study on several active cool stars including ϵ Eri. The authors used the LSD code of Kochukhov et al. (2010) to analyze spectra of this star which was observed over the course of 11 nights. Kochukhov et al. (2011) plot LSD Stokes profiles for three of these nights, and they also find that the mean longitudinal magnetic field of ϵ Eri varies between -5.8 ± 0.1 G and 4.7 ± 0.1 G over these 11 nights. As a test of our LSD code, we have used the same observations (same reduced spectra, see Kochukhov et al. 2011 for details) and line list (provided by O. Kochukhov) to extract the LSD Stokes profiles using our code. Figure 1 shows a comparison between our results and those of Kochukhov et al. (2011). We also find that the mean longitudinal field varies between -5.5 ± 0.1 G and 4.4 ± 0.1 G over the course of the 11 nights. We also analyze the null spectrum (see below) from each of the 11 nights and find longitudinal field strengths that range from -0.3 ± 0.2 G to 0.5 ± 0.2 G, and which are consistent with zero field detection on each night as expected. The agreement between results obtained with our code and that

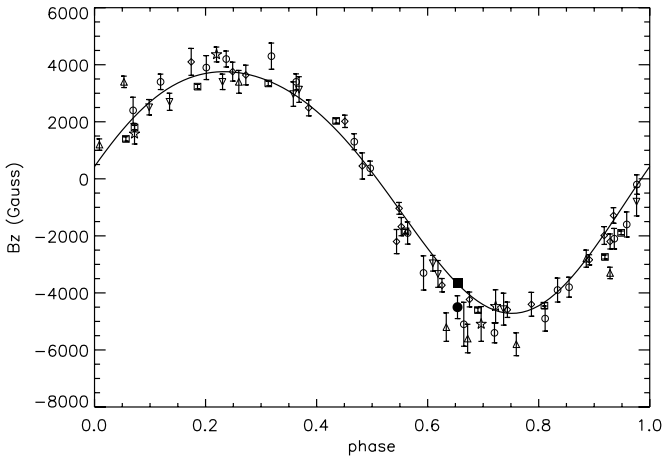

Figure 2. Longitudinal magnetic field measurements of 53 Cam. Different symbols represent different measurements by previous studies: triangle: Preston & Stepien (1968); open circles: Borra & Landstreet (1977); open star: Hildebrandt et al. (1997); open diamond: Hill et al. (1998); open square: Wade et al. (2000b); upside town triangle: Bagnulo et al. (2001); filled circle: our result, -4.5 ± 0.4 kG using 18 lines with the COG method; filled square: our result, -3.65 ± 0.08 kG using the LSD method with the integral method (the error bar is buried in the symbol itself). The solid line is the published ephemeris from Bagnulo et al. (2001). As is shown, our result is very consistent with other measurements.

of Kochukhov et al. is quite good, suggesting that our LSD code behaves similar to current state of the art LSD codes.

3.5.2. Polarization Efficiency

53 Cam is among the best studied Ap Stars with known periodic variations in its longitudinal field strength (e.g., Bagnulo et al. 2001) and has been used to test the efficiency of the ZA used with 2dcoudé before (Daou et al. 2006). We have one observation of 53 Cam on 1999 April 20 composed of one pair of exposures (one without the 1/2-wave plate in place, and the second with it in place) which is suitable for obtaining reliable polarization measurements (e.g., Donati et al. 1997). Phasing this observation according to the ephemeris of Hill et al. (1998):

$$\mathrm{JD} = 2448498.186 + 8\overset{\mathrm{d}}{.}02681E, \qquad (17)$$

we compute a phase of 0.657, at which time the mean longitudinal field is expected to be -3.75 kG according to the magnetic curve from Bagnulo et al. (2001) shown as a solid line in Figure 2. We constructed a list of 530 lines from VALD and used our LSD code to extract the intrinsic Stokes I and V profiles, which are then used to calculate the mean longitudinal field using the integral method. The mean longitudinal field we measure is -3.65 ± 0.08 kG, which is consistent with the published ephemeris. As shown in Figure 2, this result, plotted as a filled square, lies right on the magnetic curve. The uncertainty is relatively small so the error bar is buried in the symbol.

However, one concern about applying the LSD method to 53 Cam is that the weak field approximation LSD methods rely on is not valid for this star according to Wade et al. (2000a), who pointed out that there is an upper limit of around 1 kG for the weak-field regime on Ap Stars. Therefore, we then used a method that does not rely on this approximation, the integral method. We manually picked 18 spectral lines that appear well isolated and which are listed in Table 2 and used the integral method on these individual lines to measure B_z. The results from these individual lines were then averaged to obtain a final B_z measurement of -4.6 ± 0.4 kG. This result

Table 2
Line List FOR 53 Cam

ElmIon	Wavelength (Å)	Landé g Factor	ElmIon	Wavelength (Å)	Landé g Factor
Ti 2	4395.03	1.07	Fe 1	5281.79	1.18
Cr 2	4558.65	1.16	Cr 2	5313.56	1.03
Cr 2	4565.74	0.72	Cr 2	5334.87	0.41
Cr 2	4588.20	1.06	Ti 2	5418.75	1.04
Fe 1	5065.02	0.87	Fe 2	5432.97	0.29
Fe 2	5169.03	1.33	Ca 1	5594.46	1.16
Ti 2	5185.90	0.89	Fe 1	5615.64	1.19
Fe 2	5197.58	0.67	Si 2	5978.93	1.17
Fe 2	5234.62	0.87	Fe 2	5991.38	0.80

is plotted in Figure 2 as a filled circle. Due to its relatively large uncertainty, this measurement is less than 2σ away from the curve, and is therefore consistent with both the expected value from the magnetic curve and the result from the LSD method. Also plotted are measurements from several previous studies, and these are also consistent with our measurements. These measurements indicate that the polarization level we find from our instrument is in good agreement with previous studies. Similarly good agreement for the instrumentation we use was found by Daou et al. (2006). This suggests that the ZA used with 2dcoudé yields reliable measurements when circular polarization is present. Clearly, there is no evidence that the ZA suffers substantial polarization inefficiency which would produce substantial underestimates in the field.

3.5.3. Main Sequence Cool Stars and Null Tests

As an additional test of our instrumental setup, we observed a few cool stars in addition to BP Tau and 53 Cam. While some cool stars have had polarization signals detected on them, they are generally quite weak, and are expected to be much less than the signals we are looking for on BP Tau and also much less than the uncertainties we expect for the field measurements on BP Tau due to the faintness of this T Tauri star. As a result, the cool stars serve largely as null tests to ensure that our instrumental setup and analysis procedure does not produce strong spurious polarization measurements. The log of observations for these stars is given in Table 1.

As described in Donati et al. (1997) and Bagnulo et al. (2009), accurate polarization measurements can generally be made by taking a pair of observations in which the sense of polarization in the two beams is reversed as described in Section 2. If two pairs (four exposures) are obtained, accurate polarization measurements can be made, and the data from the four exposures can also be combined in such a way as to provide a null spectrum which should yield zero polarization signal even when one is really present in the data. For some of our cool star exposures, we obtained two pairs of exposures, and for others we obtained only one pair. We begin by looking at ξ Boo A (G8V), a cool star that has been studied extensively using polarimetry (Borra et al. 1984; Hubrig et al. 1994; Plachinda & Tarasova 2000; Petit et al. 2005; Morgenthaler et al. 2012), and one for which we have two pairs of observations covering a total of 6 nights. From each subexposure we get a pair of spectra, one left circularly polarized spectrum (L) and one right circularly polarized spectrum (R) or position-wise one top (T) and one bottom (B) on the CCD detector; between two subexposures, an achromatic $1/2$ wave plate is taken in/out to reverse the sense of circular polarization (exposures were made in the order of out, in, in, out for the $1/2$ wave plate). We can then combine the exposures to estimate

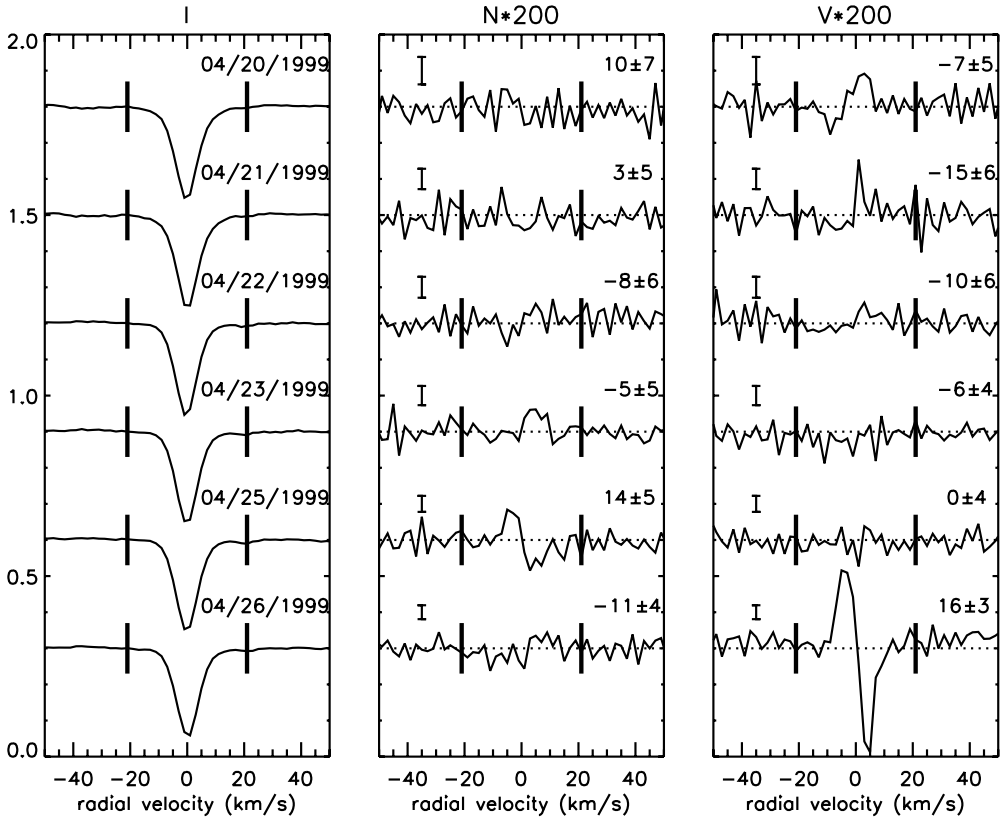

Figure 3. LSD Stokes I and V and null profiles of ξ Boo A with 2 km s^{-1} bins. Observation UT dates and B_z measurements in G are shown as text in the plots. The bold vertical lines indicate the boundaries of Stokes profiles used for integration. Stokes V and null profiles have error bars plotted to the upper left of every single profile.

Table 3
Measurements on Sun, Arcturus, 61 Cyg A and ξ Boo A (2 km s^{-1} bins)

Star	JD (2400000+)	Null (G)	N FAP	Field (G)	V FAP
Sun	50776.644	···	···	-2 ± 5	0.003
Arcturus	51149.029	···	···	-11 ± 4	1.0×10^{-8}
61 Cyg A	51288.980	11 ± 3	7.0×10^{-11}	-8 ± 5	6.5×10^{-9}
	51293.980	5 ± 2	3.1×10^{-6}	-10 ± 2	1.7×10^{-10}
	51294.985	···	···	-5 ± 3	0.00
ξ Boo A	51288.826	10 ± 7	0.30	-7 ± 5	0.020
	51289.928	3 ± 5	0.085	-15 ± 6	0.0018
	51290.970	-8 ± 6	0.26	-10 ± 6	0.84
	51291.926	-5 ± 5	0.32	-6 ± 4	9.7×10^{-4}
	51293.661	14 ± 5	1.5×10^{-9}	0 ± 4	0.088
	51294.933	-11 ± 4	3.6×10^{-4}	16 ± 3	0.00

Stokes V using:

$$4V = (R1 - L2) + (R2 - L1) + (R3 - L4) + (R4 - L3) \quad (18)$$

or equivalently

$$4V = (T1 - T2) + (B2 - B1) + (T3 - T4) + (B4 - B3). \quad (19)$$

Forming Stokes V in this way, we then used our LSD code to extract the mean Stokes V profiles for each night of observation of ξ Boo A and measured the mean longitudinal field value using the integral method. We have performed LSD analysis with velocity bins of 2 km s^{-1}. The LSD Stokes I, V, and null (see below) profiles are shown in Figure 3, and the resulting B_z and null field measurements are given in Table 3.

Equations (18) and (19) give the Stokes V spectrum; however, the data can be combined as follows to generate a null Stokes spectrum:

$$4N = (R1 - L1) + (R2 - L2) - (R3 - L3) - (R4 - L4). \quad (20)$$

or

$$4N = (B1 - T1) - (B2 - T2) + (B3 - T3) - (B4 - T4). \quad (21)$$

When analyzed with the LSD code in the same way as the Stokes V spectrum, the null should give no signal and no significant B_z measurement. Table 3 includes the results for such null tests along with the field measurements for ξ Boo A, and the null profiles are shown in Figure 3.

All of the null measurements are consistent with zero within the 3σ limit. The FAP values of these null profiles indicate similar results: no signal is detected for the first four nights, while there is one detection on 1999 April 25 and one marginal detection on the following night. These are likely spurious signals. However, these spurious signals likely do not pose any problem in establishing the zero point for BP Tau since they would be completely buried in the noise of its spectra and remain undetected: the highest amplitude of these spurious signatures is $5 \times 10^{-4}\ I_c$ while the noise level for the BP Tau LSD profiles are in the order of $10^{-3}\ I_c$. Secondly, the most accurate observations of this star are those of Petit et al. (2005) and Morgenthaler et al. (2012) where values of B_z range from -3 G to 22 G with a typical value being $\sim$8 G. Our measurements contain only one actual detection at greater than the 3σ level (16 ± 3 G) that is fully consistent with previous results.

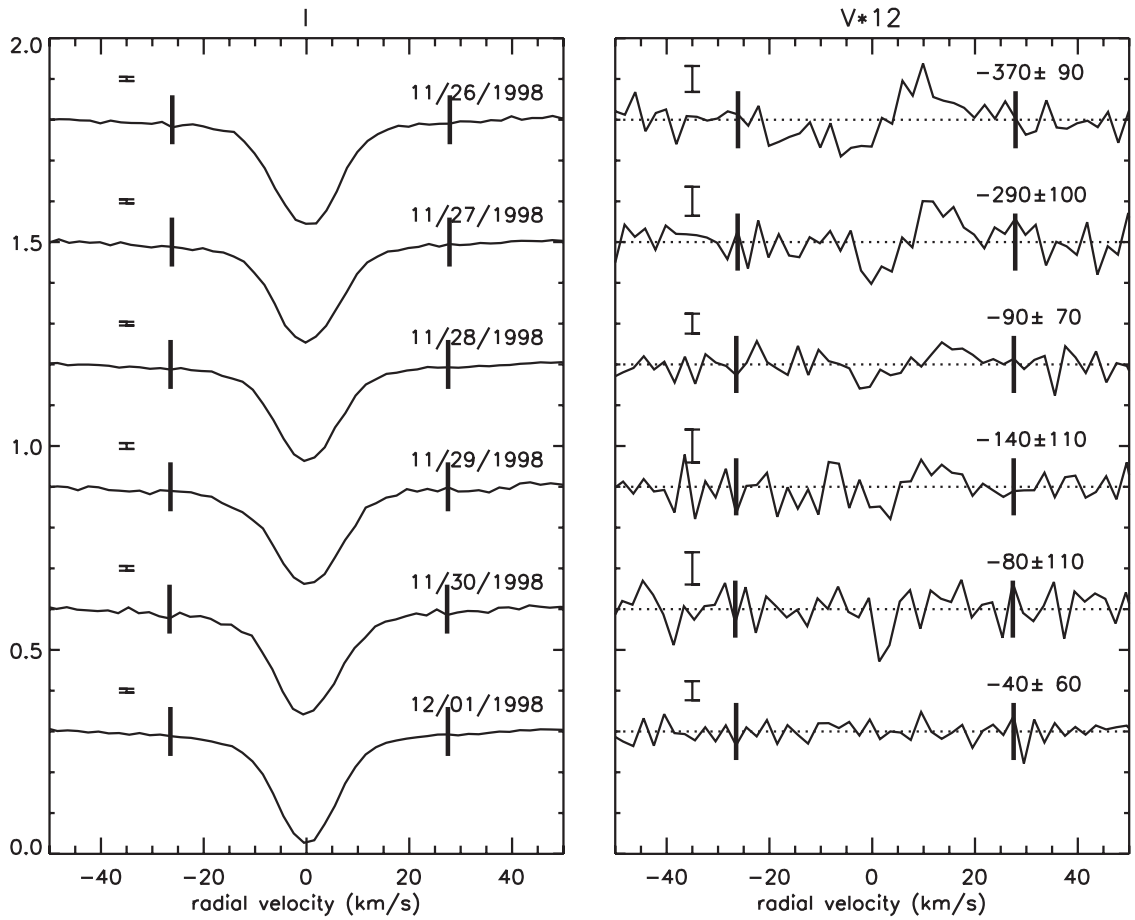

Figure 4. LSD Stokes *I* and *V* profiles of BP Tau. Symbols and texts are used in the same way as in Figure 3.

In addition to ξ Boo A, we also observed the Sun (by observing the asteroid Vesta), Arcturus, and 61 Cyg A. In the case of the Sun and Arcturus, and one of the observations of 61 Cyg A, only one pair of spectra were obtained. However, since the true polarization of these stars is expected to be quite small, we can still analyze these stars and verify that indeed our recovered signals are small or zero within the uncertainties. This method of verifying that there are no significant sources of spurious polarization signals is often used by investigators in the field (e.g., Donati et al. 1997; Wade et al. 2000a). The Sun and Arcturus were both observed by Wade et al. (2000a) with no detection of polarization at levels below our final uncertainties. The K5V star 61 Cyg A has been studied by Tarasova et al. (2001) who measure a maximum magnitude for the longitudinal field of $B_z = -13.8 \pm 3.2$ G. Most of their 12 observations of this star were consistent with zero field with uncertainties typically of 2–3 G. Our field measurements for these three stars are given in Table 3 where the B_z measurements are quite low and mostly consistent given our observational uncertainties. On two nights, we have two pairs of observations for 61 Cyg A and so are able to also form a null spectrum, which are also reported in Table 3. The FAP indicates that weak spurious signals do exist in the spectra of these two nights. However, as discussed above in the case of ξ Boo A, the spurious signals are again quite weak and would be undetectable in the spectra of BP Tau. All three of these test stars are very slow rotators and their lines are unresolved at the observed resolution. Therefore, to judge the level of uncertainty errors in establishing the zero point of the velocity scale may produce in our longitudinal field analysis, we can simply look at the strength of the B_z measurements derived from the null spectra. These are generally 10 G or lower, and again all but one is consistent with zero field within the measured uncertainties. Such a small zero point offset does not affect the derived uncertainties in our BP Tau measurements which are considerably larger due to the lower S/N of these data. All of these tests on cool stars suggest that our instrumental setup and analysis technique are generally robust enough against spurious polarization signals in Stokes *V* that are strong enough to affect our study on BP Tau. They also suggest that our estimated uncertainties are realistic. We perform one final test of this with data from BP Tau described below.

3.6. Photospheric Measurements for BP Tau

We follow the procedures described above to measure the mean longitudinal magnetic field on BP Tau. A total of 375 lines with central depths greater than 0.2 (after rotationally broadening) were chosen. Regions with too many strong lines blended together are also excluded. Including the strongly blended regions introduces more noise in the derived LSD profiles. Figure 4 shows the obtained LSD Stokes *I* and *V* profiles which are scaled to the mean values of the wavelengths, Landé-*g* values, and central depths of the lines used (6072.5 Å, 1.34, and 0.420, respectively). The results are included in Table 4 and Figure 5.

Since we have only one pair of observations of BP Tau on each night, we can get reliable polarization measurements (e.g., Donati et al. 1997; Bagnulo et al. 2009), but we are not able to recombine the right and left components to get a proper null spectrum to analyze. However, we can still perform a null

Table 4
Mean Longitudinal Magnetic Fields on BP Tau in G

JD (2400000+)	Photospheric Lines	False Alarm	Telluric Lines	False Alarm	He I 5876 Å	Ca II Average
51143.722	-370 ± 90	7.88×10^{-7}	10 ± 40	0.14	3500 ± 300	1400 ± 140
51144.628	-290 ± 100	3.79×10^{-4}	-10 ± 40	0.44	1400 ± 300	900 ± 130
51145.647	-90 ± 70	5.47×10^{-2}	-10 ± 30	0.50	400 ± 300	670 ± 120
51146.635	-140 ± 110	0.298	70 ± 50	0.50	900 ± 400	350 ± 160
51147.670	-80 ± 110	6.69×10^{-2}	-70 ± 60	0.51	400 ± 500	-220 ± 200
51148.644	-40 ± 60	0.628	10 ± 60	0.41	700 ± 300	350 ± 100

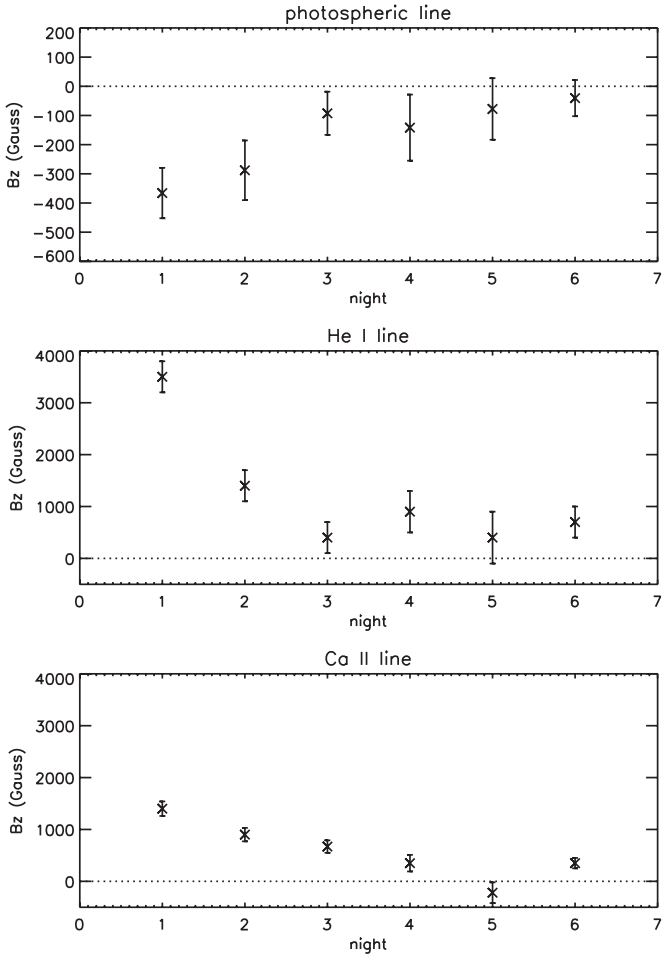

Figure 5. Mean longitudinal magnetic field measurements on BP Tau. The bottom panel shows the average of the two members of the Ca II triplet.

test using telluric lines observed in the spectrum. Telluric lines are not expected to show any circular polarization due to the weakness of the Earth's magnetic field. Thus, we can analyze these lines in exactly the same way as we analyze the stellar lines to provide a check on potential spurious polarization signals. In addition, this has the advantage that we combine the spectra in exactly the same way as we do when analyzing the stellar lines, where as the null spectra discussed in Section 3.5.3 are combined differently than in the case for the true polarization measurement. For this telluric test, we constructed a line list of 40 lines spanning the wavelength range 6800–7700 Å. The line depths (needed for the LSD analysis) assigned to each line are the actual depths in the observed spectra. In addition, we need to assign a Landé-g value for the lines to convert our measurements into a longitudinal field value. We assign the same Landé-g value to each of the telluric lines, using the mean Landé-g determined from the photospheric absorption lines used to analyze BP Tau. We then use our LSD code to analyze these telluric lines and determine B_z values in the same way as done for the photospheric lines. These telluric null field values are reported in Table 4. The resulting Stokes I and V profiles are shown in Figure 6. The measured B_z values are small and within 1σ of 0 G and the false alarm probabilities are all greater than 10^{-3}, indicating again that the instrument does not generally produce spurious polarization signals that affect our BP Tau observations and that our uncertainty estimates are appropriate. The reader will note that the uncertainty estimates from these telluric lines are generally smaller than those determined from analyzing the photospheric lines, even though there are more lines used in the photospheric analysis compared to the telluric analysis. The reason for this is that most of the photospheric lines used are fairly weak, and so add relatively little to the sensitivity, while the telluric lines are all quite strong and therefore provide much greater sensitivity.

4. EMISSION LINES

Emission lines of T Tauri Stars often show strong polarization, which is also the case for BP Tau (e.g., Johns-Krull et al. 1999a). Shifts between left and right circularly polarized spectra are clearly seen. Our observations cover three strong emission lines, He I (5876 Å) and Ca II (8498 Å and 8542 Å) that are known to show polarization. These three lines are often characterized as having a broad component and a narrow component (NC; e.g., Edwards et al. 1994; Batalha et al. 1996). The two Ca II lines display broad photospheric absorption components with emission in the core, while the He I line has a broad emission feature with additional narrow emission on top of this. We extract the NCs by first fitting second order polynomials to the broad features and subtract them from the original observed spectra (Figure 7). Figure 8 shows the Stokes I and V profiles of the NCs of these three emission lines. We then use the integral method (e.g., Donati et al. 1997; Wade et al. 2000b) to calculate the mean longitudinal fields from these profiles. Results are given in Table 4 and shown in Figure 5.

5. DISCUSSION

Zeeman broadening measurements of the mean magnetic field strength on the stellar surface are available for many TTSs, including BP Tau. Strong, kilogauss fields have been widely detected on these TTSs. Table 3 in Johns-Krull (2007) lists mean magnetic field measurements for 15 TTSs, most of which are above 2 kG. In the case of BP Tau, the mean field strength is 2.1 kG. Similar studies have been carried out by several other authors as well (e.g., Yang et al. 2008; Yang & Johns-Krull 2011), and similar results are obtained.

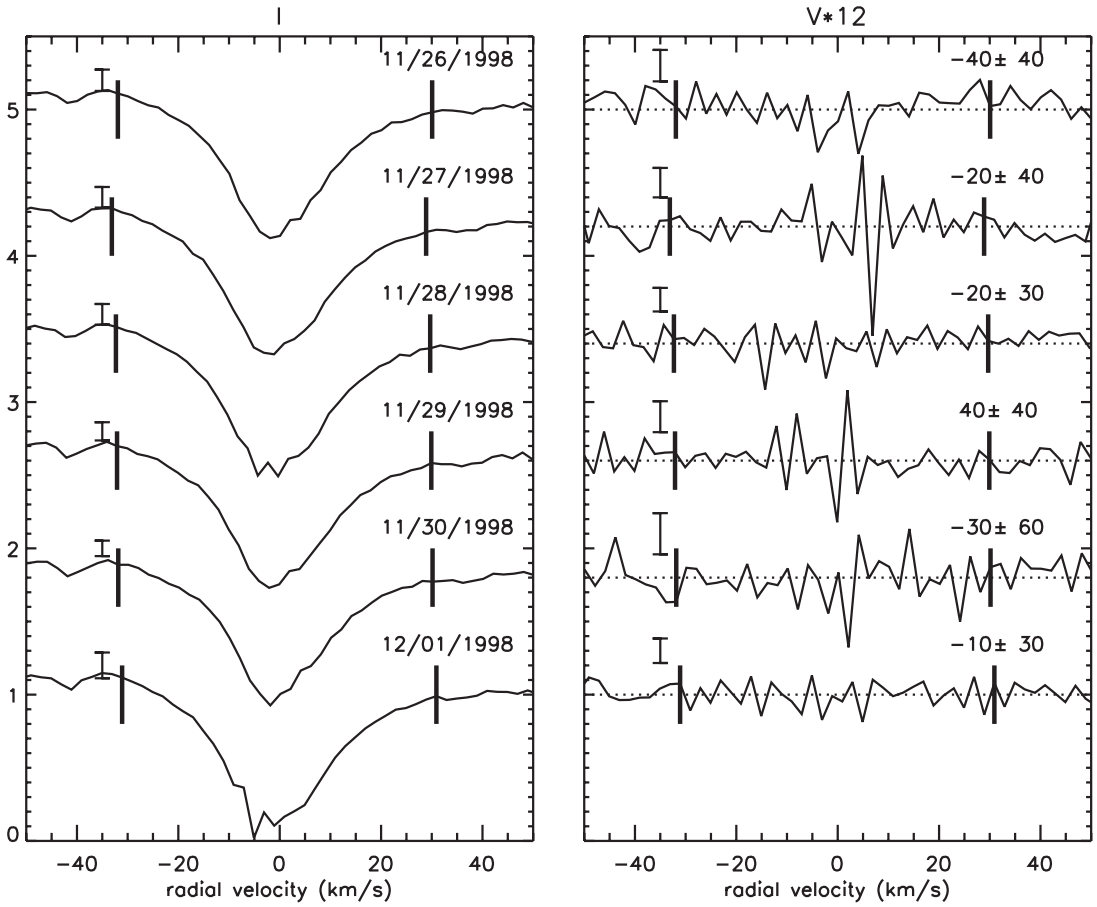

Figure 6. LSD Stokes *I* and *V* profiles of BP Tau telluric lines. Symbols and texts are used in a similar way as Figure 3.

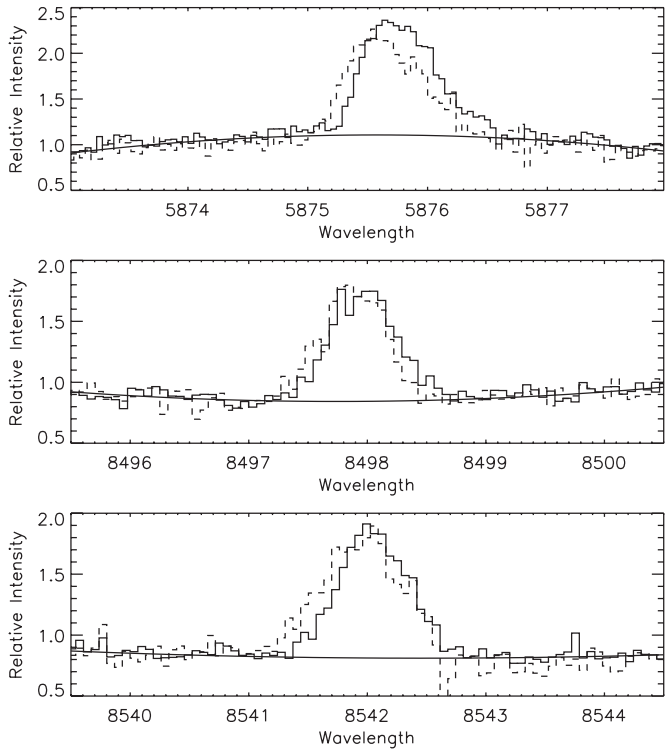

Figure 7. Sections of observed spectra for three different emission lines, He I 5876 Å and Ca II 8498 Å and 8542 Å. Solid histograms are the right circularly polarized components, and dashed histograms are the left circularly polarized components. The solid line is a second polynomial fit to the broad components of these lines.

Zeeman broadening measurements provide limited information on the magnetic field geometry. Spectropolarimetry studies can provide geometric information, though they provide only a lower limit to the mean field strengths. From our high-resolution ($R \approx 60{,}000$) right and left circularly polarized spectra taken on six consecutive nights which cover almost an entire rotational period (8.31 days for BP Tau; Xiao et al. 2012), we measured the mean longitudinal magnetic field on BP Tau. No fields with a magnitude greater than 370 G are found from the photospheric lines, while fields measured from the three emission lines are much higher, on the order of a kG or more.

Spectropolarimetry studies of the mean longitudinal magnetic fields of BP Tau and other CTTSs have been carried out in the past. A common conclusion from the work here and in many of these studies is that mean longitudinal fields measured from emission lines and mean fields measured by using Zeeman broadening of photospheric lines are very strong, on the order of several kG; while measurements of mean longitudinal fields from photospheric lines are significantly weaker. Johns-Krull et al. (1999a) studied BP Tau, and from the He I 5876 Å emission line they measured a field stronger than 2 kG. They also used four unblended magnetically sensitive Fe I lines and found a mean longitudinal photospheric field of -40 ± 50 G, so fields stronger than 200 G were ruled out at the 3 σ level. Valenti & Johns-Krull (2004) studied four TTSs (AA Tau, BP Tau, DF Tau, and DK Tau), and again kilogauss fields are detected in the emission line regions (He I 5876 Å) while from photospheric lines most of the field measurements are around 100 G (see their Figures 5 and 6) or less. Symington et al. (2005) studied the same emission line (He I 5876 Å) on seven TTSs, three of

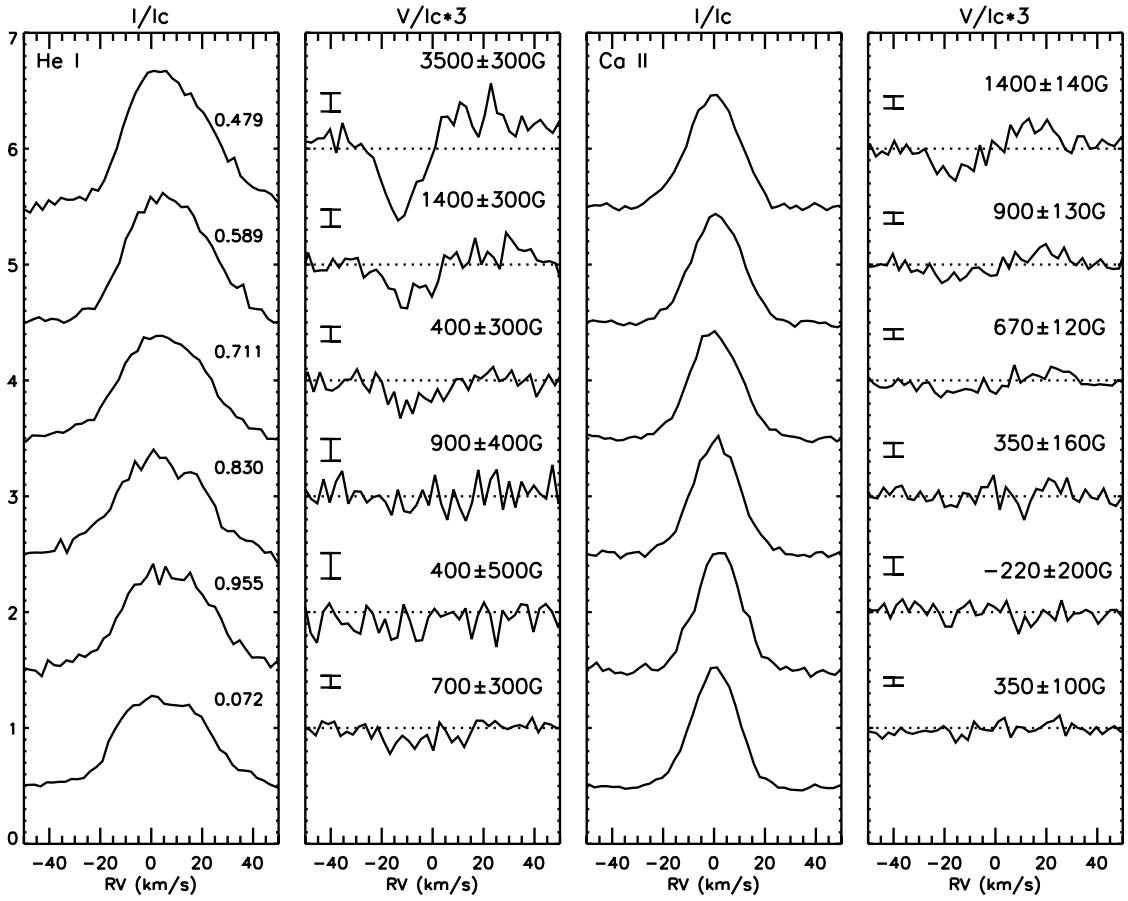

Figure 8. Stokes *I* and *V* spectra for the narrow components of emission lines of BP Tau, He I 5876 Å (left two), and Ca II 8498 Å and 8542 Å averaged (right two).

which (BP Tau, DF Tau, and DN Tau) had strong fields detected. On BP Tau they detected a peak field of 4.4 ± 1.2 kG. Yang et al. (2007) observed the CTTS TW Hydrae on six nights. In their analysis, they used 12 isolated photospheric absorption lines with relatively large Landé *g*-factors and cross-correlated their left circularly polarized and right circularly polarized line profiles to measure the separation and then the longitudinal fields, which were averaged to get the final longitudinal field measurements. Except on one night where they obtained a field of 149 ± 33 G, no mean longitudinal fields stronger than 100 G were found with a typical uncertainty of 50 G. However, polarization was clearly found in the emission lines He I (5876 Å) and Ca II (8498 Å), which yielded a weighted mean field of −1673 ± 50 G for the He I line and −276 ± 19 G for the Ca II line. An interpretation of these results is that small scale strong magnetic fields are present on the surface of these TTSs. However, integrating over the whole stellar surface cancels out much of these small-scale strong fields, leaving only a significantly reduced longitudinal field as diagnosed by the photospheric absorption lines. For the emission lines showing strong polarization, their formation regions are believed to be the base of the accretion footpoints which cover only a small fraction of the stellar surface, allowing these emission lines to show very strong polarization, indicative of the smaller scale field. This is consistent with modified versions of magnetospheric accretion models (e.g., Mohanty 2009). It is clear that spectropolarimetric observations are inconsistent with a purely dipole field geometry aligned with the stellar rotation axis (Johns-Krull et al. 1999a; Daou et al. 2006; Yang et al. 2007; Donati et al. 2007, 2008, 2010).

5.1. Mean Longitudinal Field

As already mentioned above, with one observation, Johns-Krull et al. (1999a) used four unblended magnetically sensitive Fe I lines which form over the entire stellar surface and measured a mean longitudinal field of −40±50 G, so fields with a magnitude larger than 200 G were ruled out at the 3σ level for this one particular observation. Valenti & Johns-Krull (2004) reported similar results. On the other hand, Donati et al. (2008) analyzed two sets of time series of spectropolarimetric observations of BP Tau (full phase coverage for one set and almost full phase coverage for the other, 17 observations in total) and measured photospheric fields ranging from −60 G to −600 G with uncertainties ranging from 40 G to 140 G, using a similar LSD technique as described in this paper. They used a total of 9400 lines with central depths greater than 0.4 when no non-thermal broadening mechanism is present. While there is a discrepancy between the interpretation of Donati et al. (2008) and Johns-Krull et al. (1999a), the observations themselves are fully consistent with each other given the quoted uncertainties and the variations reported by the former. Donati et al. (2008) argue that the different interpretations might result from either temporal variations of BP Tau (data for Johns-Krull et al. (1999a) were taken in 1997 and the two sets of data for Donati et al. (2008) were taken in 2006, with one set in February and the other in November and December) or the use of cross-correlation methods by Johns-Krull et al. (1999a), which Donati et al. (2008) argue tend to underestimate both the mean longitudinal fields and the error bars, instead of the integral method or equivalents as used in Donati et al. (2008). In this paper, our observations

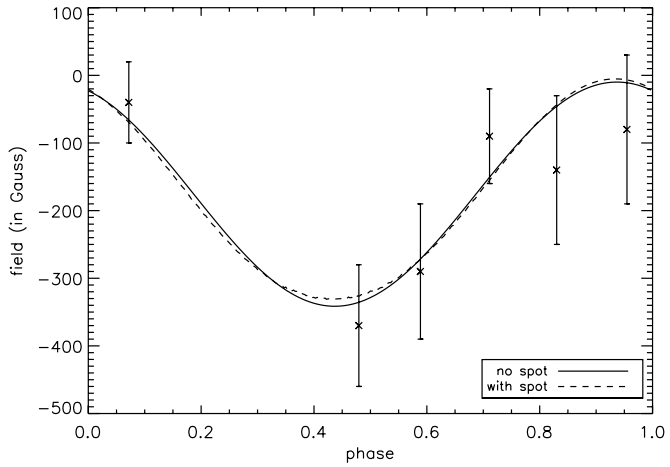

Figure 9. Dipole fittings with (dashed line) and without (solid line) a spot to the time series of our photospheric measurements (crosses with error bars) of BP Tau.

were taken on six consecutive nights in 1998, covering almost a full rotation, and a similar LSD method as used by Donati et al. (2008) is used to extract the Zeeman signatures. We find mean longitudinal fields with magnitudes no greater than 370 G, with uncertainties below 100 G. These results tend to agree with Johns-Krull et al. (1999a) better than they do with Donati et al. (2008). Therefore, using cross-correlation methods is probably not the main reason why the two sets of measurements appear different, though as mentioned above, the measurements are in fact not necessarily inconsistent with each other.

Donati et al. (2008) assumed an inclination of 45° for the rotation axis of BP Tau in their analysis of the star. The measurements of B_z from the photospheric lines reported here can be fit with a model of a dipole magnetic field with the dipole axis misaligned with respect to the stellar rotation axis. As described below, the dipole component is by far the dominant contributor to the net field on the stellar surface, and Donati et al. (2008) find a strong dipole component on BP Tau. If the stellar inclination of 45° is adopted, the simple misaligned dipole model yields the fit shown by the solid line in Figure 9. The Marquardt method (Bevington & Robinson 1992) is used in this fit. Here, the dipole axis is tilted at an angle of $137° \pm 10°$ with respect to the rotation axis and the polar field strength is 1050 ± 220 G.

The above fit assumes that the entire stellar surface contributes to the value of B_z determined from the photospheric absorption lines. However, it is likely that not all of the stellar photosphere actually contributes to the lines we observe. Dark star spots and accretion hot spots are generally believed to not contribute to optical photospheric absorption lines because in the first case, for cool spots, the local surface flux on the star is simply too faint relative to the nonspotted regions, and in the second case, the temperature in the accretion zones is too hot ($\sim 10^4$ K or more) to produce the same photospheric lines seen from these cool stars. For example, Donati et al. (2008) assumed that the photospheric lines form only from the nonaccreting regions of the stellar surface, which they took to be coincident with the spotted regions of the star. Such an accretion zone can affect the photospheric value of B_z that a model predicts since some (magnetic) regions of the star will not contribute to the spectral lines from which B_z is measured. For a dipole field geometry, a spot at the magnetic pole will have the largest impact since it will block the regions of the star with the strongest local field from contributing to B_z. We gauge the potential magnitude of this effect of removing some portion of the photosphere that contributes to the absorption line profiles on the resulting Bz values by repeating the fit above, but this time including a dark spot on the magnetic poles which covers 5% of the projected stellar surface (this blockage of the stellar photosphere in terms of the effect on photospheric line profiles can be compared to the 2% accretion filling factor derived by Donati et al. (2008) or the 6.4% accretion filling factor found by Valenti et al. 1993). This new model fit is shown in Figure 9 in the dashed line. The parameters of the fit (dipole field strength of 1200 ± 260 G with a tilt angle also of $136° \pm 10°$) are very similar to those derived without the spot, due simply to the fact that accretion zones on CTTSs cover a relatively small portion of the stellar surface. Both dipolar field models yield similar mean fields of about 900 G, which is inconsistent with the observed 2.1 kG mean field. It is almost certain at this point that the surface field configurations on BP Tau as well as many, or even all other, CTTSs are not purely dipolar. More complicated field geometries could be similar to the small-scale structures dominating at the surface of the Sun, which can be expanded to different order components such as dipole, quadrupole, octupole, etc. However, higher order magnetic field components fall off more rapidly with increasing distance from the star than lower order field components. Therefore, it is quite likely that at the inner disk edge, which is several stellar radii away from the star, the dipole component is already dominating, and accretion is still governed by this dipole component. This may well explain the smooth night-to-night variation of the longitudinal fields measured from the emission lines found in this and several other studies.

Generally, higher order components from a spherical harmonic expansion contribute much less to the longitudinal field component than lower order terms. For example, assuming polar fields are all unity in arbitrary units, a dipole field reaches its maximum mean longitudinal field strength of 0.324 when viewed pole on assuming 0.6 for the limb darkening coefficient, while the maximum a quadrupole can reach is 0.058 and an octupole 0.022. Therefore, if not at some extreme viewing angle, the information from mean longitudinal field measurements will be dominantly from the dipole component, which makes time series of mean longitudinal field measurements a good diagnostic of this component of the field.

5.2. Stokes Profile Model Fit

While mean longitudinal field measurements can give some information on the magnetic field geometries on stellar surfaces, various more sophisticated field imaging packages have been developed (Kochukhov et al. 2004; Donati et al. 2007) which try to fit the actual Stokes V profile. However, these packages have similar requirements in order to successfully recover a surface field image. First, the object needs to rotate fast enough so that components on the stellar disk with different projected radial velocities (shown as stripes on a stellar disk parallel to the projection of the rotation axis) can be distinguished from each other in the spectra. Since a rotationally broadened line is a convolution of the local intrinsic profile and a rotation pattern, different segments of the line wings (different wavelength displacements from the line center) correspond to components with different projected radial velocities on the stellar disk if the intrinsic profile is sufficiently narrow. Second, high-resolution spectrographs are needed so that different segments of the line

Table 5
Model Fit Results

Models	Dipole			Octupole			Spot	Filling	χ_r^2
	B_p	θ	ϕ	B_p	θ	ϕ	Size	Factor	
1	180 ± 30	106 ± 11	0.542 ± 0.026				0%	0%	2.19
2	240 ± 30	113 ± 9	0.534 ± 0.021	250 ± 70	117 ± 8	0.616 ± 0.019	0%	0%	2.17
3	2440 ± 220	140 ± 3	0.619 ± 0.021	4950 ± 550	122 ± 4	0.707 ± 0.029	0%	25%	2.01
4	1850 ± 110	130 ± 4	0.598 ± 0.011	1400 ± 150	105 ± 4	0.708 ± 0.010	0%	25%	1.97

profile can be resolved. These two requirements provide spatial resolution on the stellar disk. Third, the fields should be stable within the rotation cycles that the observations cover. Fourth, time-series observations of Stokes profiles (at least Stokes I and V profiles) are available. These two provide temporal resolution for the imaging process. According to previous studies, BP Tau is a moderate rotator with a $v\sin i$ of about 10 km s^{-1}, which is actually low for Doppler imaging based studies (e.g., Vogt et al. 1987). Nevertheless, investigators have been attempting Doppler imaging based studies on BP Tau and other stars with similar $v\sin i$ values. With the high-resolution spectropolarimetric data we obtained which cover almost a full rotation period, we should at least be able to investigate the plausibility of some of the magnetic models.

The goal then is to model the resulting LSD Stokes I and V profiles. We assume a Voigt profile for intrinsic local line profile and a Gaussian instrumental broadening corresponding to the resolution of the instrument used for this study (∼60,000). We further assume a Zeeman triplet as the splitting pattern for this intrinsic line, whose wavelength and Landé-g value are set to be 6072.5 Å and 1.34, respectively, the average for the lines used to construct the LSD profiles (the final LSD Stokes profiles have been scaled to these same values). For rotational broadening, we adopt a $v\sin i$ of 10 km s^{-1}. We then perform a fit to the time-series Stokes I profiles to search for the best values for the free parameters of the Voigt profile along with the relative veilings for each night. Veiling is a quantity that describes how much the spectrum of a star, more precisely, the absorption lines, are affected by the contributions to the stellar continuum by emissions from accretion spots. Higher veiling means more accretion emission and shallower absorption lines. It can vary from night to night. We set relative veiling to be zero for the night when the final profile has the deepest line and then fit the ones for other nights.

Many Zeeman Doppler imaging codes reconstruct a magnetic map for the surface of the star and then fit a spherical harmonic expansion to the resulting image. Instead, our code first assumes a certain geometry (combinations of different components of spherical harmonic expansions such as dipole, quadrupole, octupole) with certain parameters (polar field B_p, inclination of the magnetic axis with respect to the rotation axis, θ, and azimuthal position of the magnetic pole at phase zero ϕ), and we find the best fit values for these parameters of the spherical harmonics. For a given set of parameters, Stokes I and V profiles can be computed. We then use the Marquardt method (Bevington & Robinson 1992) to determine the best values for the parameters by fitting the extracted intrinsic Stokes I and V profiles for the six nights shown in Figure 4. As a check on whether the code is working properly, we compute the mean unsigned field strength and the mean longitudinal field together with the Stokes profiles. These field values are then compared with the ones determined from the analytical expressions for multipole field geometries (dipole, quadrupole, octupole, etc.) using expressions derived in Gregory et al. (2010, see also Schwarzschild 1950).

Donati et al. (2008) carried out a detailed investigation on the magnetic field geometry on BP Tau. They found that the field topology predominantly consists of a 1.2 kG dipole and a 1.6 kG octupole, both slightly tilted with respect to the rotation axis, which itself is inclined by 45° with respect to the line-of-sight. A dark spot coincident with accretion shock regions and covering 8% (actually 2% considering an assumed filling factor of 0.25—see below) of the stellar surface is present and located close to the magnetic poles. The concept of a filling factor was introduced to provide better fits to the wings of the Stokes V profiles. A filling factor of ψ means that only a fraction, ψ, of the stellar surface is actually covered by magnetic fields and the other $1 - \psi$ of the surface contains no fields and so does not contribute to the polarization level in Stokes V. During the modeling, they found that a filling factor of 0.25 gives a reduced χ^2 of 1, and only filling factors that are significantly smaller than unity are able to fit the Stokes profiles within the noise level, especially in the far wings. The dipole and octupole strengths quoted above refer to the magnetic flux. Thus, the field in these regions must be multiplied by 4 to account for the filling factor.

We attempted to reproduce this field geometry, but we were not able to obtain a good fit to our observed Stokes profiles in Figure 4 using it: Zeeman signatures in LSD Stokes V profiles have opposite polarities with a reduce χ^2 of 2.795. Therefore, we perform our own fitting for the parameters described above using our observed Stokes I and V profiles as constraints. All of the results for different models are shown in Table 5 and Figure 10. To start with, since a purely dipole model, with its axis aligned with the rotation axis, is not able to produce any variation in the observed Stokes profiles, we first fit the Stokes LSD profiles using a dipole tilted at some angle (a free parameter) with respect to the rotation axis (Model 1). We allow for a dark spot on the surface which does not contribute to the total flux at all but find that the spot size is driven toward 0% of the surface area for the best fit while the Stokes I profiles are reproduced well. Therefore, a spot does not appear to be required to reconstruct the Stokes I profiles we obtained. The fit for the Stokes V profiles, on the other hand, is not as good: the profiles of the first two nights clearly show much stronger magnetic signatures than those of the following four nights, and the model tends to fit the latter much better, leaving the strong signatures on the far ends of the wings for the first two nights poorly matched (the model does not produce signatures strong or broad enough compared to the data—if it did, the polarization near the center of the line would be much too strong and the fit for the last 4 nights would be substantially worse). Parameters that directly affect this are the stellar $v\sin i$ and the strength of the magnetic field. Since a $v\sin i$ of ∼10 km s^{-1} or less has been confirmed by different authors who get consistent values (e.g., Johns-Krull et al. 1999b; Johns-Krull & Valenti 2001; Donati et al. 2008), it is unlikely that the $v\sin i$ could be in error (too low)

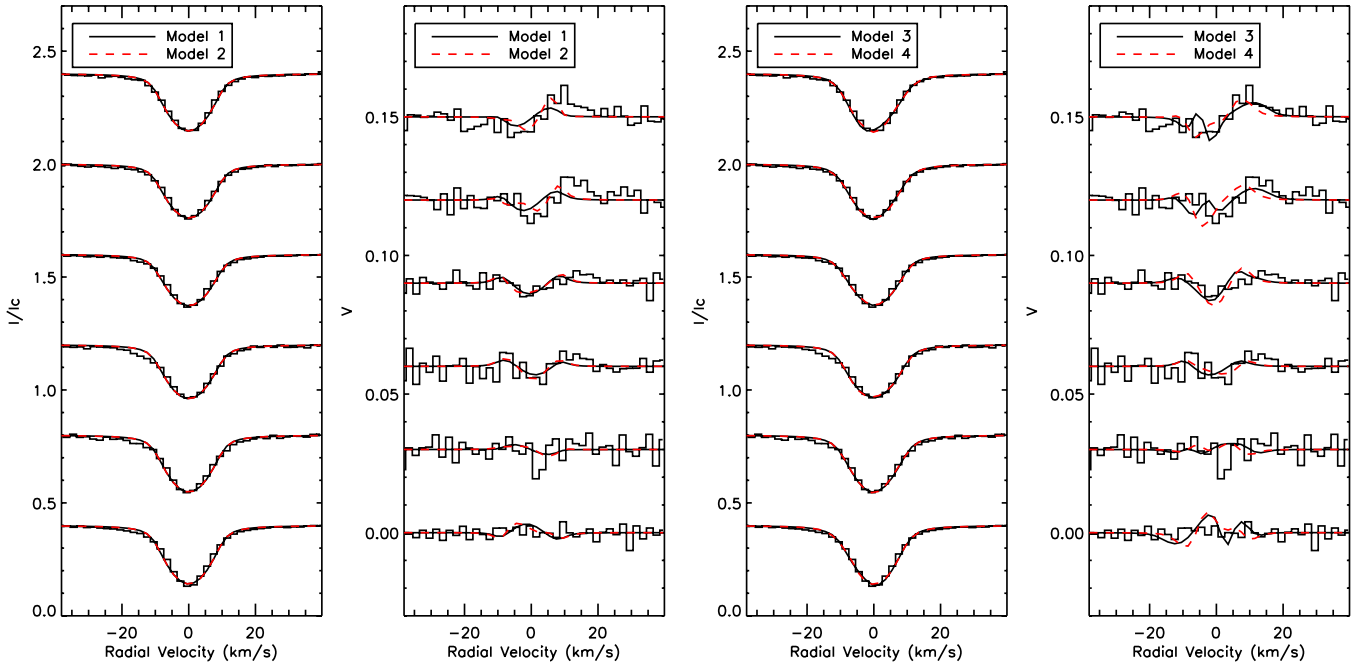

Figure 10. Stokes *I* and *V* fits for different models described in Section 5.2. Parameters for the models are shown in Table 5. Model 1 is a dipole with a potential spot which turned out to be not necessary; Model 2 is a combination of a dipole and an octupole with a possible spot; Model 3 has both a dipole and an octupole with a possible spot, and in each cell on the stellar surface, only 25% is covered by large scale magnetic field while the other 75% is not; Model 4 has the same as Model 3 except that outside the 25% that is covered by large-scale magnetic field there are small-scale field structures that only contribute to the broadening of Stokes *I* profile, not to polarization. In the left two panels, the black solid line is for Model 1 and the red dashed line is for Model 2; in the right two panels, the black solid line is for Model 3 and the red dashed line is for Model 4.

(A color version of this figure is available in the online journal.)

by enough to remedy this. Another option then is to increase the field strength present on the star.

The above solution found the best fit including only a dipole component. One way to increase the field strength in the fit is to add another higher order field component such as quadrupole, octupole, or higher order field. Higher order fields tend to generate magnetic signatures further in the wings and contribute less to the mean longitudinal field than a dipole with a similar polar field strength. Since Donati et al. (2008) found predominantly a dipole and an octupole, we added an octupole component to our model (Model 2). Again the best fit spot size is driven toward a filling factor of 0. Compared with the results of the dipole only fit, the dipole plus octupole fits Stokes *I* similarly well, while the signatures in Stokes *V* are indeed stronger in amplitude but they still do not extend far enough in the line wings. It is this same behavior that led Donati et al. (2008) to include a filling factor to the field itself (see above). In principle, this allows fields with larger strengths to be present on the stellar surface without increasing the magnetic flux. Since the overall flux can remain low, there can be minimal affect on Stokes *I* while the signal in Stokes *V* can move further out into the line wings. We tried magnetic filling factors of 25%, 50%, and 75%, obtaining the best fits for 25% as found by Donati et al. (2008). With this filling factor (Model 3), we recover a much stronger field in the magnetic regions (a 2.5 kG dipole plus a 5.2 kG octupole which translate to 630 G and 1.3 kG, respectively, in terms of magnetic flux once the 25% filling factor is accounted for), and we are able to reproduce the Zeeman signatures in the far wings. Again, the spot size in drive to zero.

As discussed above, the success of fitting the LSD Stokes profiles appears to depend on the inclusion of a filling factor for the large scale magnetic fields. For example, Donati et al. (2008) use a filling factor of 0.25. We too find a better fit by assuming a filling factor of 0.25 for the large-scale field. A filling factor less than unity implies even stronger magnetic fields are present in order to produce a given level of polarization. For example, Donati et al. (2008) find field strengths extending up to 10 kG in their analysis of BP Tau; however, the fields cannot be arbitrarily strong and maintain pressure equilibrium with their surroundings. This fact then permits constraints on the fields present at the surface of the star. Due to their lower surface gravity, the gas pressure in the photosphere of TTSs can balance only relatively weak magnetic fields, at least compared to that present on the Sun's surface (Safier 1998, 1999; Johns-Krull et al. 1999b; Rajaguru et al. 2002). For the case of BP Tau, the maximum field strength that can be present in the photosphere is ∼1.0 kG (Johns-Krull et al. 1999b) if gas pressure in the surrounding nonmagnetic quiet atmosphere is responsible for maintaining pressure equilibrium with the magnetized regions. This fact has lead to the conclusion that essentially the entire surface of TTSs must be confined with strong magnetic fields in order for pressure balance to be maintained (Safier 1999; Johns-Krull et al. 1999b, 2004; Johns-Krull 2007; Yang et al. 2005, 2008), and Donati et al. (2008) suggest that the atmosphere of BP Tau outside the 25% they find is contributing to the observed polarization and is filled with small-scale magnetic fields which can maintain the pressure equilibrium but do not contribute to the polarization because the small spatial scale results in nearly complete flux cancellation. Therefore, we also tried a model fit where in each surface area element of the star we included the same 25% containing the large-scale field of the dipole plus octupole components, while in the remaining 75% we assumed there are small-scale magnetic fields which do not contribute to polarization in the Stokes *V* profiles but which do produce line

broadening that can affect the Stokes *I* profile (Model 4). It is realized as follows: 25% of a stellar surface grid is covered by a large-scale dipole field and 75% covered by small-scale fields; the field strength in the 75% was set equal to the field in 25% so that pressure balance is maintained; when calculating the contribution of this 75% of the grid to the final right and left circularly polarized spectra (*R* and *L*), we use the local Stokes *I*, i.e., $(R_{\rm loc}+L_{\rm loc})/2$ for both *R* and *L* so that it contributes to the broadening of the Stokes *I* profiles but not the Stokes *V* profiles. Compared with Model 3, this model yields lower polar field strengths but the resulting fits for both Stokes *I* and *V* profiles are of similar quality. The mean field strength from Model 4 is about 1.3 kG. Model 4 produces the overall best reduced χ^2 value of all the models we tried. This model contains a 1.85 kG dipole (magnetic flux of 0.46 kG) plus a 1.40 kG octupole (magnetic flux of 0.35 kG).

The χ_r^2 values for all of these models is close to 2 and there is relatively little difference between them. The fact that these χ_r^2 values are significantly larger than 1 suggests that either the profile uncertainties have been underestimated or that there are missing pieces to the model needed to properly fit the data. We have restricted the model to only two dominant multipolar components, so it would not be surprising if there are indeed missing components. The uncertainties in the LSD Stokes profiles have been estimated by looking at the continuum regions in the final profiles, and are therefore unlikely to be significantly underestimated, though we return to this point below. To determine how significant the difference in the fits between the four models is, it is necessary to examine χ^2, not its reduced form. When estimating confidence intervals in multidimensional fits, error ellipses are usually drawn around the χ^2 minimum where χ^2 is increased by some specified value of $\Delta\chi^2$, with this region enclosing some percentage of the likely solutions. Here, we have six free parameters, so the appropriate value of $\Delta\chi^2$ is 7.04 to enclose 68.3% (1σ) of the likely solutions (Press et al. 1986). Since we are fitting a total of 480 line profile points (the Stokes *I* and *V* profiles over the 6 nights), this corresponds to a change in reduced χ^2 of $\Delta\chi_r^2 = 0.015$. This suggests that Model 4 is better than Model 3 at the 2.7σ level and is better than Model 2 at the 13.3σ level. The χ_r^2 of the model with no magnetic field is 4.00, which is 135σ worse than Model 4. Since the best χ_r^2 is about 2 instead of 1, it is fair to increase the uncertainties by a factor of 2, in which case these significance levels come down by a factor of 2. Artificially increasing the observed uncertainties until χ_r^2 is 1.0 is often done in the magnetic imaging community as a means of distinguishing between models as described above (e.g., Donati et al. 2008).

5.3. Stokes I Profile

As discussed above, the introduction of a filling factor well below unity allows strong magnetic fields to be present which enables much wider Stokes *V* signatures to be produced without producing correspondingly strong Stokes *V* signatures near line center. This can reproduce the features in the far wings of the observed Stokes *V* profiles. However, strong fields as high as several kG, such as found in Model 3 and by Donati et al. (2008), are unphysical if they occupy only a small filling factor on the surface of the star since the gas pressure in the non-magnetic regions is too small to balance the magnetic pressure induced by such strong fields. If these "the non-magnetic regions" are covered by small-scale magnetic fields, which maintain pressure balance between two regions but do not contribute to the polarization due to local polarity cancellation, the strong fields do not pose a problem from the point of view of pressure balance. However, these small-scale fields could show up in Stokes *I* measurements. Model 4 took this into account; however, stronger fields than are found here have been suggested for BP Tau.

Donati et al. (2008) find that the average magnetic flux in regions contributing to the photospheric polarization (i.e., outside the accretion and dark spots on the surface) is 1.2 kG which corresponds to a field strength of 4.8 kG for BP Tau. In order to maintain pressure balance across the stellar surface, this then implies a mean magnetic field of about 4.8 kG on the stellar surface, substantially in excess of the mean field of 2.2–2.6 kG found from observations of magnetically sensitive *K* band Ti I lines (Johns-Krull et al. 1999b; Johns-Krull 2007). Our implementation of their dipole plus octupole model described in Section 5.2 predicts a somewhat lower value, but still quite high. In Figure 11, we show again in the left panel the observed Stokes *I* profiles for all our BP Tau observations along with predicted Stokes *I* profiles for a model with a 4.8 kG dipole plus a 6.4 kG octupole with a dark spot blocking 2% of the stellar surface near the pole where the field is the strongest. This represents the distribution of magnetic field strengths over the surface of the star that would result from the Donati et al. (2008) model when the quiet regions are filled with small-scale magnetic fields that balance magnetic pressure that results from their recovered large-scale fields which fill only 25% of each surface area element. The right panel shows the mean magnetic field outside of the spotted region as a function of rotation phase. While Donati et al. (2008) find a mean field outside this spotted region of 4.8 kG (their 1.2 kG *flux* multiplied by 4 to account for the filling factor), we find an average value of ~3.8 kG using only the dipole plus octupole components. Our value is similar in magnitude; however, it is likely lower because we do not include the smaller scale components present in the Donati et al. (2008) image reconstruction. Nevertheless, as we see in the left panel of Figure 11 and additionally below, this lower field strength is still too strong to match the observations. The Stokes *I* profiles in this figure clearly show that the predicted line profiles are too broad compared to the observed LSD *I* profiles.

As discussed in Section 3.4, concern is sometimes raised over LSD analyses because they rely in principle on complete and accurate line lists, and it is usually the case that the line lists used are neither complete or 100% accurate. In the case of such strong fields; however, LSD analysis is not required to meaningfully constrain the mean magnetic field strength in the photosphere. The Fe I 8468.40 Å line is a good diagnostic of magnetic fields in cool stars (e.g., Johns-Krull & Valenti 1996; Johns-Krull 2008; Phan-Bao et al. 2009) due to its high Landé-*g* value (2.5) and its relatively long wavelength in the optical band pass. Mean fields of the strength found in Figure 11 should produce a noticeable affect on this line, even at the lower S/N that results when not using LSD. We boost the S/N in this line in BP Tau by averaging our observations over all six nights, obtaining a profile with a S/N ~ 100. Since we are using a time averaged line profile, we then also only compare to the mean magnetic field strength present on BP Tau at this time. In order to analyze this line, we perform detailed spectrum synthesis of the line profile. We take initial values for the required line data from VALD (Kupka et al. 1999). As with all detailed spectral line analysis, it is often necessary to verify the atomic parameters of the specific line(s) to be analyzed, and a common way to do so (e.g., Valenti & Piskunov 1996) is to compare synthetic spectra of the lines to the NSO Solar Atlas (Kurucz et al. 1984), which is the method we follow here.

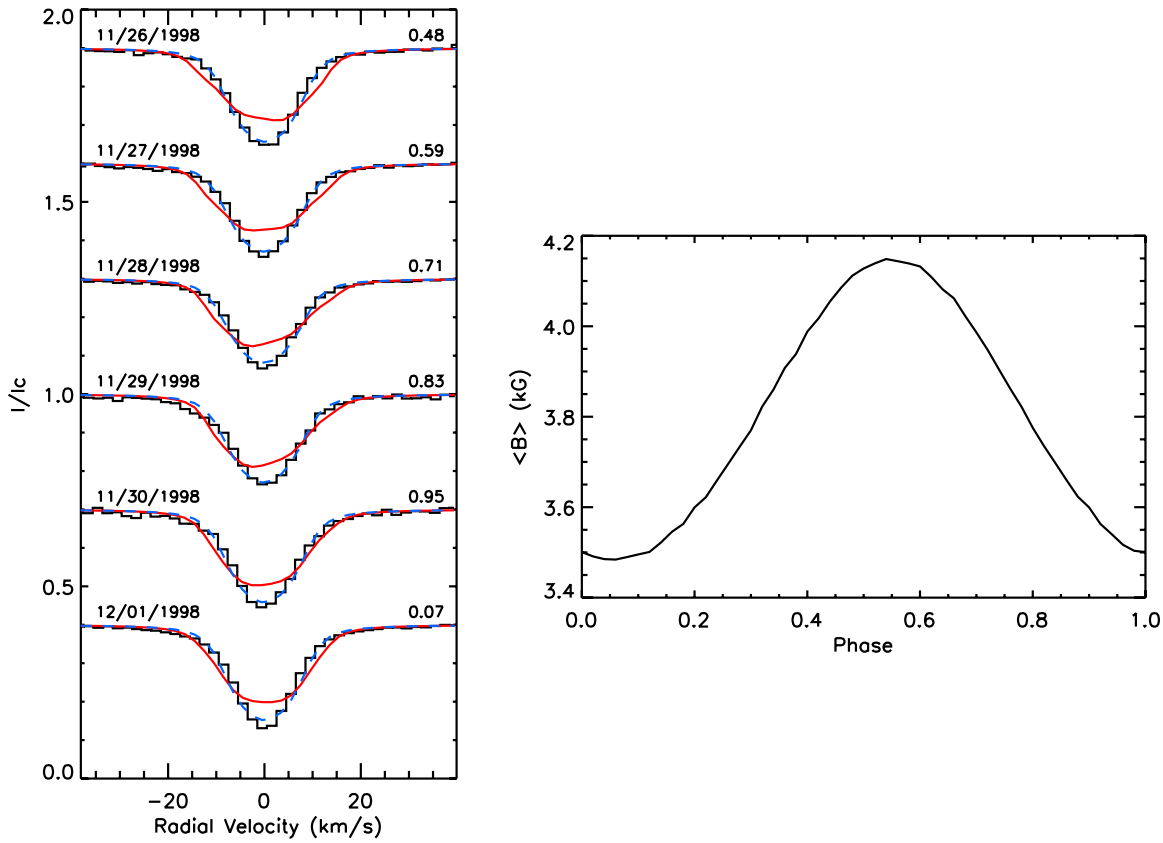

Figure 11. Left-hand panel shows the observed time series of LSD Stokes *I* profiles for BP Tau in the solid histogram. The smooth red solid curve shows the predicted Stokes *I* profiles from a combined dipole plus octupole field model similar to that proposed by Donati et al. (2008) but with a filling factor of 1.0 instead of 0.25, which is shown as the blue dashed line. Profiles are marked with their observing dates and corresponding rotation phase values. The filling factor of 1.0 takes into account magnetic fields with small-scale spatial structure which are required to provide pressure balance with the large scaled fields proposed by Donati et al. The small-scale fields do not contribute to the polarization observed in Stokes *V*; however, their signature remains in Stokes *I*, producing line profiles that are noticeably broader than the observed profiles. These profiles include the effects of accretion and dark spots covering ∼2% of the stellar surface in the highest field regions which do not contribute to the photospheric profiles as found by Donati et al. The right-hand panel shows the disk averaged unsigned magnetic field strength (the field modulus) as a function of rotation phase for this model.

(A color version of this figure is available in the online journal.)

At the cool temperatures associated with BP Tau and most other TTSs, VALD (Kupka et al. 1999) predicts this line to be a very close blend with a Ti I line at 8468.47 Å. Therefore, additional care must be taken when checking/determining atomic line parameters from the Solar Atlas. Fortunately, the two lines have somewhat different behavior with temperature, and in both the Sun and in K7 stars, the Fe I line is predicted to dominate the observed spectral line (Kupka et al. 1999 and below). In order to provide additional constraints on the atomic data in the 8468 region, we synthesize spectra of both the Sun (using the Solar Atlas for comparison) and 61 Cyg B (using the $R = 121{,}000$ spectrum described in Section 2 for comparison). The K7 star 61 Cyg B has the same spectral class and a similar effective temperature as BP Tau and therefore serves as a good probe of the behavior of these spectral lines at the appropriate stellar parameters. We again use SYNTHMAG to synthesize the final spectra, but with a zero magnetic field for both stars. For the Sun, we used an interpolated Kurucz ATLAS9 (Kurucz 1993) model atmosphere interpolated to the best fitting solar parameters as given by Valenti & Piskunov (1996) for the case where van der Waals damping (γ_6) is enhanced by a factor of 2.5 relative to the Unsöld (1955) approximation. For 61 Cyg B, we use the model atmosphere determined for this star by Johns-Krull et al. (1999b) which is a NextGen model atmosphere (Allard & Hauschildt 1995) interpolated to stellar parameters appropriate for the star. Figure 12 plots the 8468 Å region of both the Sun and 61 Cyg B, showing the observed spectra as well as the final fitted synthetic spectrum for both stars. Also shown are individual spectrum syntheses of the Fe I 8468.40 Å and Ti I 8468.47 Å lines using the final atomic parameters which shows the relative contribution of the two lines to the final profile. We use the Marquardt method to simultaneously solve for the best fitting gf values for both of these lines using both the observed solar and 61 Cyg B spectra as constraints. At the same time, we also solved for the van der Waals broadening term for the Fe I 8468.40 line. We attempted a run where we also solved for the van der Waals broadening term for the Ti I 8468.47 line; however, the value of this parameter was driven very low in the fit, so we hold it fixed at the original value returned by VALD. Finally, we solved for both the gf and van der Waals terms for the weaker Ti I line at 8467.14 Å because this line is fairly prominent in this region of the BP Tau spectrum, and it is also fairly magnetically sensitive.

Examining Figure 12 shows that the final fitted line parameters are able to simultaneously produce synthetic spectra in good agreement with the observed spectra of the Sun and 61 Cyg B for the 8468.4 Å line. The line parameters for the two lines that make up this feature changed by relatively small amounts: the equivalent width of the Fe I 8468.40 Å line increased by 12% for the 61 Cyg B synthesis, while the Ti I 8468.47 Å line equivalent

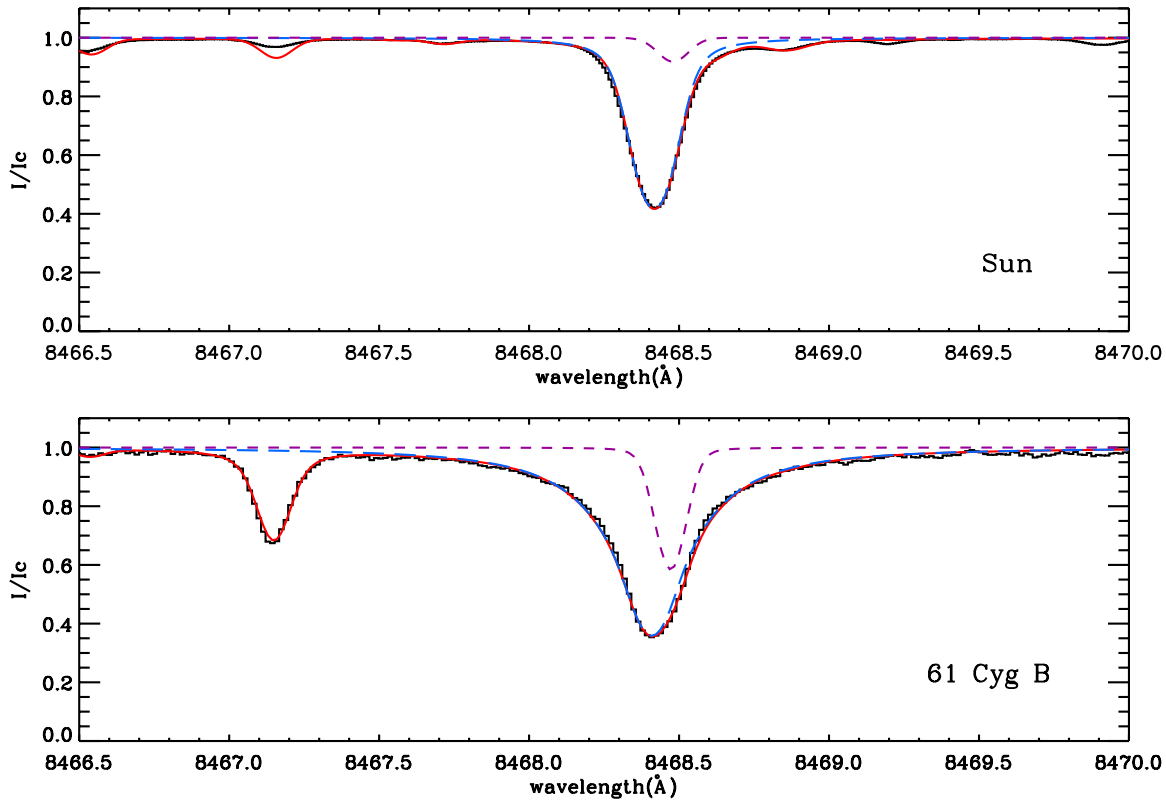

Figure 12. Top panel shows the solar spectrum (Stokes *I*) in the neighborhood of the Fe I 8468.4 Å line in the solid histogram. The final synthetic fit is shown in the smooth solid red curve, while the blue long-dashed curve shows the synthesis of only the Fe I 8468.40 Å line and the short-dashed purple curve shows the synthesis of only the Ti I 8468.47 Å line. The bottom panel shows the same for the K7V star 61 Cyg B. The loggf values of these two 8468 Å lines as well as the van der Waals broadening term of the Fe I 8468.40 Å line were determined by simultaneously matching these spectra. In addition, the loggf and van der Waals broadening terms for the Ti I line at 8467.15 Å were determined by fitting these observed spectra.

(A color version of this figure is available in the online journal.)

decreased by about 17%. No other lines overlapping with this feature within 0.15 Å are predicted by VALD to have a depth greater than 0.001. The fit for the Ti I 8467.14 Å line is not as good, likely due to an unknown blending line or lines that is/are unaccounted for in the spectrum synthesis. It is not uncommon for there to be weak lines present in the spectrum which do not appear in line lists such as VALD. For example, the solar spectrum of Figure 12 shows a weak line at ~8469.90 Å for which there is no line in the VALD database that is predicted to appear with a depth greater than 0.001 in the spectrum of a star with solar parameters. There is also a weak line in the observed solar spectrum at a wavelength of ~8469.20 Å, and while lines near this wavelength appear in the VALD database with a predicted strength greater than 0.001, the identification of this line is not clear. We speculate that there is an additional unknown line that blends with the line at 8467.14 Å, and as a result, the parameters we derive for this Ti I line are in error, which leads to our inability to simultaneously fit this feature in the spectrum of both the Sun and 61 Cyg B. On the other hand, since the spectrum synthesis does a good job matching the spectra of the 8468.4 Å feature with only small corrections to the line parameters required, we are confident in our ability to model this feature in the spectra of BP Tau.

As mentioned above, Donati et al. (2008) suggest that the entire surface of BP Tau is covered with a magnetic field whose average strength is 4.8 kG in order to maintain pressure equilibrium with the 25% of the star which contains the large-scale field they measure in their polarization analysis. In our estimation of a similar model, we find an average field strength of 3.8 kG. We can then estimate effects of such a strong field on the 8468.4 Å feature by synthesizing spectra of this region in the presence of a magnetic field. We again use the line synthesis code SYNTHMAG (Piskunov 1999) and assume for simplicity a radial magnetic field at the surface. We use the detailed line splitting patterns for the Fe I 8468.40 Å and Ti I 8468.47 Å lines calculated with LS coupling. We use the model atmosphere of Johns-Krull et al. (1999b) for BP Tau which is a NextGen model (Allard & Hauschildt 1995) interpolated to the parameters appropriate for BP Tau. As a check, we also used a NextGen model with $T_{\rm eff} = 4000$ K, $\log(g) = 3.5$, and [M/H] = 0.0 and found no significant difference with the profiles synthesized from the BP Tau model atmosphere. The top panel of Figure 13 shows the results of the spectrum synthesis, using fields of both 3.8 and 4.8 kG, compared to the observed mean line profile of BP Tau in the 8468.4 Å region. In fitting the synthesized profiles to the observations, we allowed for a continuum veiling as a free parameter and held $v\sin i$ fixed at 10.2 km s^{-1} as found by Johns-Krull et al. (1999b). The top panel of this figure shows that the synthesized 8468.4 Å feature is clearly too broad for either field value compared to the observations, while the synthetic profile with no magnetic field is too narrow. We then let the field strength be a free parameter along with the veiling and again fit the observed 8468.4 Å feature or BP Tau. The best fits are shown in the bottom panel of Figure 13. We performed two such fits, one holding the $v\sin i$ fixed at 10.2 km s^{-1} as found by Johns-Krull et al. (1999b) and one with $v\sin i$ held fixed at 9.0 km s^{-1} as found by Donati et al. (2008). The two synthetic profiles are virtually indistinguishable, and as expected, the

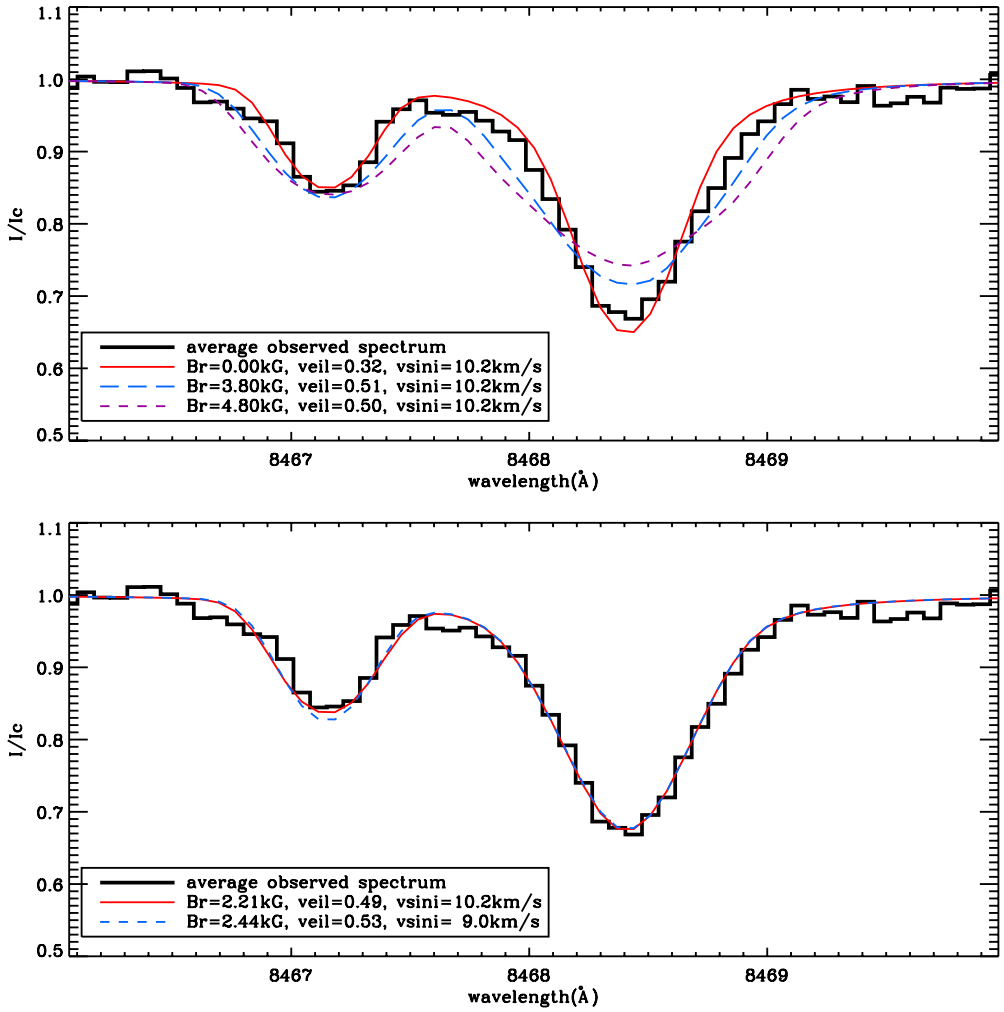

Figure 13. Both panels show the average spectrum (Stokes *I*) of BP Tau in the neighborhood of the Fe I 8468.4 Å line in the solid histogram. In the top panel, the smooth red curve shows the synthetic spectrum with no magnetic field. The long-dashed blue curve shows the synthetic spectrum with an assumed radial magnetic field of 3.8 kG. The short-dashed purple curve shows the synthetic spectrum with an assumed radial field of 4.8 kG. In all three cases, veiling was used as a free parameter to fit the profiles to the observations, and the resulting veiling values are given in the figure legend. Clearly, the profiles with these strong fields are too broad while the profile with no magnetic field is too narrow by a small amount. The bottom panel shows synthetic profiles when both the strength of the radial magnetic field and the veiling are treated as free parameters. The smooth, solid red curve shows the resulting profile when holding the $v\sin i$ fixed at 10.2 km s^{-1}, giving a resulting magnetic field strength of 2.3 kG. The dashed blue curve shows the resulting profile when holding the $v\sin i$ fixed at 9.0 km s^{-1}, giving a resulting magnetic field strength of 2.5 kG.

(A color version of this figure is available in the online journal.)

higher $v\sin i$ yields a somewhat lower magnetic field of 2.2 kG while the lower $v\sin i$ yields a higher field of 2.4 kG. Both of these field strengths agree well with the mean fields derived from IR Zeeman broadening measurements (2.6 ± 0.3 kG by Johns-Krull et al. 1999b and 2.2 ± 0.2 kG by Johns-Krull 2007), and they are substantially weaker than the mean field implied by Donati et al. (2008). The veilings derived in these fits ($\sim$0.5) are fully consistent with the veilings in this spectral region found by previous investigators (e.g., Basri & Batalha 1990). Thus, it appears that the very strong mean field *strengths* on BP Tau implied by the Donati et al. (2008) analysis are not present in our data or in the published infrared studies of this star. On the other hand, the mean fields we determine in a fit to this line are more than strong enough to account for the best fit model we obtain for our Stokes *V* data (Model 4 of Table 5). In fact, that fit produces a mean magnetic field of only 1.3 kG, implying that the large-scale field likely has an even smaller filling factor and stronger field strength; however, the regions not covered with large scale field must still be magnetic based on pressure equilibrium.

5.4. Emission Lines

Yang et al. (2007) reported different levels of polarization between the He I 5876 Å emission line and the Ca II 8498 Å line on TW Hya and argued that this is probably due to different contributions to the lines from different line forming regions. For the Ca II lines, the NC of the emission line is present both in TW Hya and NTTSs but with different equivalent widths (EWs: 0.69–0.98 Å for TW Hya and 0.53–0.59 Å for the 7 NTTSs studied by Batalha et al. 1996). This suggests the existence of both a chromospheric contribution and another, likely accretion related, contribution. It is generally thought that chromospheric emission occurs wherever fields pierce the surface of the Sun outside of cool spots, and this likely happens on other cool stars as well. We might then expect that the polarization and implied value of B_z in chromospheric lines will be similar to that seen in photospheric lines. On the Sun, we expect to see rapid field fall off into the chromosphere as the field lines expand with height due to the small filling factor of field in the photosphere where it can be confined by the gas pressure. In the case of T

Tauri Stars, the mean field measurements show that essentially the entire surface of the star is covered with fields which are stronger than can be confined by gas pressure, so this field decline with height may well not occur in the chromosphere on these young stars. In this case, polarization in accretion zones may be diluted by chromospheric polarization for lines like Ca II that have significant contributions from both regions. For the He I line, the EWs of the NCs range between 0.00 and 0.09 Å for the NTTSs studied by Batalha et al. (1996) and are 2.5 to 4.3 Å for TW Hya indicating the contribution to the He I line from the chromosphere is probably quite limited, allowing the polarization level for this line to remain high. Yang et al. (2007) also predicted that the other two members of the Ca II triplet (not covered by their observations) should show similar levels of polarization because the members of this triplet should form in the same regions. Our observations reproduce these results, this time for BP Tau instead of TW Hya. As seen in Table 4 and Figure 8, the level of polarization of the He I line is about twice as high as the Ca II lines, and we obtained similar mean longitudinal fields from the two Ca II lines covered by our observations. Similar observational results are obtained by Donati et al. (2007, 2008); however, Donati et al. (2008) do not allow for the possibility that chromospheric emission is polarized in their interpretation of the results.

6. SUMMARY AND FUTURE WORK

The primary goal of this paper is to study magnetic properties of BP Tau. All of the tests performed for the LSD procedure and the instrumentation serve as validation checks on this primary goal. Spectropolarimetric data for this study were obtained at the 2.7 m Harlan J. Smith Telescope at McDonald Observatory using the Zeeman analyzer and cross-dispersed coudé echelle spectrometer (Vogt et al. 1980; Tull et al. 1995). Objects include the Sun (by observing the asteroid Vesta), 61 Cyg A, ξ Boo A, 53 Cam, and BP Tau, with the first four being test stars and the last the star of interest in this study. To analyze these spectropolarimetric echelle data reduced using the package described in Valenti (1994), we have implemented an LSD code which averages hundreds to thousands of spectral lines to effectively extract intrinsic Stokes profiles, especially Stokes *V* profiles since our objects of interest have low levels of net polarization and therefore quite weak Zeeman signatures in Stokes *V* profiles.

As tests of our LSD code, we analyze the same reduced spectra of ϵ Eri used by Kochukhov et al. (2011) and get almost identical LSD Stokes profiles compared with their LSD Stokes profiles. To establish the zero-point uncertainty of our instrumentation, we analyzed the null spectra constructed by using spectra of ξ Boo A and 61 Cyg A from two pairs of consecutive exposures. Although according to the FAP, weak spurious signals are detected in the null profiles, the amplitudes of these signals are too small to be detected in the spectra of BP Tau. The weak field measurements on these stars and the Sun are also consistent with results from previous studies. The well-studied Ap Star 53 Cam serves as a non-zero magnetic standard, on which we observed $B_z = -4.5 \pm 0.4$ kG at phase 0.657 as indicated by its magnetic rotation curve in Bagnulo et al. (2001). This shows that the polarization efficiency of our instrumentation is quite good for fields of a few kG. Field measurements using 40 telluric lines in the spectra of BP Tau also showed null results as expected, which again indicates that our system does not produce strong spurious signals in the measurements of BP Tau. Finally, applying this code to spectra of BP Tau using 375 photospheric lines yields measurements of mean longitudinal fields with the maximum amplitude of -370 ± 80 G on the first night. Our time-series LSD Stokes *V* profiles yield a best fit of a 1.8 kG dipole tilted at 129° with respect to the rotation axis and a 1.4 kG octupole tilted at 104° with respect to the rotation axis, both with a filling factor of 25%, which is also consistent with the line broadening measurements. Introducing the concept of a magnetic filling factor ψ i.e., that large scale magnetic field only cover a portion (ψ) of the stellar surface allows stronger field and enables us to explain the wide Stokes *V* profiles. However, to maintain pressure balance between the two regions of the star, we introduced small-scale fields in 1-ψ potion of the stellar surface: they are assumed small scale so opposite polarities completely cancel out and do not contribute to Stokes *V*. These small-scale magnetic fields maintain pressure balance with the large-scale field regions. Studies of the emission lines give measurements of the order of a kG, which is consistent with previous studies, as well as with mean field strengths determined from IR Zeeman broadening measurements.

After the first introduction of the least-square deconvolution method more than a decade ago, many modified methods have been developed. Sennhauser & Berdyugina (2010) developed Zeeman Component Decomposition (ZCD) and argue that ZCD overcomes limitations of the weak-field and weak-line approximations and has the advantage of applying simultaneously to all Stokes parameters. Kochukhov et al. (2010) describe their iLSD method, which uses multiple average profiles instead of one single profile as assumed in a regular LSD code, and showed an increase in the quality of extracted intrinsic profiles. In the future, we will explore how these techniques can be applied to the spectra of T Tauri Stars.

We acknowledge the support from the NASA Origins of Solar Systems grant NNX10AI53G to Rice University. This work also made use of the VALD line database and the NASA Astrophysics Data System.

REFERENCES

Allard, F., & Hauschildt, P. H. 1995, in Bottom of the Main Sequence and Beyond, ed. C. G. Tinney (Berlin: Springer), 32
Babcock, H. W. 1960, ApJ, 132, 521B
Bagnulo, S., Landolfi, M., Landstreet, J. D., et al. 2009, PASP, 121, 993
Bagnulo, S., Wade, G. A., Donati, J.-F., et al. 2001, A&A, 369, 889
Barnes, J. R. 1999, PhD thesis, Univ. St. Andrews
Basri, G., & Batalha, C. 1990, ApJ, 363, 654
Basri, G., Marcy, G. W., & Valenti, J. A. 1992, ApJ, 390, 622
Batalha, C. C., Stout-Batalha, N. M., Basri, G., & Terra, M. A. O. 1996, ApJS, 103, 211
Bevington, P. R., & Robinson, D. K. 1992, Data Reduction and Error Analysis for the Physical Sciences, 2e, ed. D. Bruflodt & S. J. Cotkin (New York: McGraw Hill), 161
Borra, E. F., Edwards, G., & Mayor, M. 1984, ApJ, 284, 211
Borra, E. F., & Landstreet, J. D. 1977, ApJ, 212, 141
Borra, E. F., & Landstreet, J. D. 1980, ApJS, 42, 421
Camenzind, M. 1990, RvMA, 3, 234
Daou, A. G., Johns-Krull, C. M., & Valenti, J. A. 2006, AJ, 131, 520
Donati, J.-F., Jardine, M. M., Gregory, S. G., et al. 2007, MNRAS, 380, 1297
Donati, J.-F., Jardine, M. M., Gregory, S. G., et al. 2008, MNRAS, 386, 1234
Donati, J.-F., Semel, M., Carter, B., Rees, D., & Collier Cameron, A. 1997, MNRAS, 291, 658
Donati, J.-F., Semel, M., & Rees, D. E. 1992, A&A, 265, 669
Donati, J.-F., Skelly, M. B., Bouvier, J., et al. 2010, MNRAS, 409, 1347D
Edwards, S., Hartigan, P., Ghandour, L., & Andrulis, C. 1994, AJ, 108, 1056
Gregory, S. G., Jardine, M., Gray, C. G., & Donati, J.-F. 2010, RPPh, 71, 126901
Hartmann, L., & Stauffer, J. R. 1989, AJ, 97, 873
Hartmann, L., Hewett, R., & Calvet, N. 1994, ApJ, 426, 669

Hildebrandt, G., Scholz, G., & Woche, M. 1997, AN, 318, 291
Hill, G. M., Bohlender, D. A., Landstreet, J. D., et al. 1998, MNRAS, 297, 236
Hubrig, S., Plachinda, S. I., Hunsch, M., & Schroder, K. P. 1994, A&A, 291, 890
Hussain, G. A. J., Collier Cameron, A., Jardine, M. M., et al. 2009, MNRAS, 398, 189
Johns-Krull, C. M. 2007, ApJ, 664, 975
Johns-Krull, C. M. 2008, in ASP Conf. Ser. 384, 14th Cambridge Workshop on Cool Stars, Stellar Systems, and the Sun, ed. G. van Belle (San Francisco, CA: ASP), 145
Johns-Krull, C. M., & Valenti, J. A. 1996, ApJL, 459, L95
Johns-Krull, C. M., & Valenti, J. A. 2001, ApJ, 561, 1060
Johns-Krull, C. M., Valenti, J. A., Hatzes, A. P., & Kanaan, A. 1999a, ApJL, 510, L41
Johns-Krull, C. M., Valenti, J. A., & Koresko, C. 1999b, ApJ, 516, 900
Johns-Krull, C. M., Valenti, J. A., & Saar, S. H. 2004, ApJ, 617, 1204
Kochukhov, O., Bagnulo, S., Wade, G. A., et al. 2004, A&A, 414, 613
Kochukhov, O., Makaganiuk, V., & Piskunov, N. 2010, A&A, 524, A5
Kochukhov, O., Makaganiuk, V., Piskunov, N., et al. 2011, ApJL, 732, L19
Kupka, F., Piskunov, N. E., Ryabchikova, T. A., Stempels, H. C., & Weiss, W. W. 1999, A&AS, 138, 119
Kurucz, R. 1993, ATLAS9 Stellar Atmosphere Programs and 2 km/s Grid. Kurucz CD-ROM No. 13 (Cambridge, MA: Smithsonian Astrophysical Observatory)
Kurucz, R. L., Furenlid, I., Brault, J., & Testerman, L. 1984, National Solar Observatory Atlas Number 1 (Sunspot, NM: National Solar Observatory)
Mathys, G. 1989, FCPh, 13, 143
Mathys, G. 1991, A&A, 89, 121
Mathys, G., & Lanz, T. 1992, A&A, 256, 169
Mohanty, S., & Shu, F. H. 2009, in Protostellar Jets in Context, ed. K. Tsinganos, T. Ray, & M. Stute (Berlin: Springer), 51
Morgenthaler, A., Petit, P., Saar, S., et al. 2012, A&A, 540A, 138
Petit, P., Donati, J.-F., Auriére, M., et al. 2005, MNRAS, 361, 837
Phan-Bao, N., Lim, J., Donati, J.-F., Johns-Krull, C. M., & Martín, E. L. 2009, ApJ, 704, 1721
Piskunov, N. 1999, Astrophysics and Space Science Library, 243, 515
Plachinda, S. I., & Tarasova, T. N. 2000, ApJ, 533, 1016
Press, W. H., Flannery, B. P., & Teukolsky, S. A. 1986, Numerical Recipes. The Art of Scientific Computing (Cambridge: Cambridge Univ. Press), 687
Preston, G. W., & Stepien, K. 1968, ApJ, 151, 583
Rajaguru, S. P., Kurucz, R. L., & Hasan, S. S. 2002, ApJL, 565, L101
Safier, P. N. 1998, ApJ, 494, 336
Safier, P. N. 1999, ApJL, 510, L127
Schwarzschild, M. 1950, ApJ, 112, 222
Sennhauser, C., & Berdyugina, S. V. 2010, A&A, 522, A57
Shu, F. H., Najita, J., Ostriker, E., et al. 1994, ApJ, 429, 781
Symington, N. H., Harries, T. J., Kurosowa, R., & Naylor, T. 2005, MNRAS, 358, 977S
Tarasova, T. N., Plachinda, S. I., & Rumyantsev, V. V. 2001, ARep, 45, 475
Tull, R. G., MacQueen, P. J., Sneden, C., & Lambert, D. L. 1995, PASP, 107, 251
Unsöld, A. 1955, Physik der Sternatmosphären (Berlin: Springer)
Valenti, J. A. 1994, PhD thesis, Univ. California, Berkeley
Valenti, J. A., Basri, G., & Johns, C. M. 1993, AJ, 106, 2024
Valenti, J. A., & Johns-Krull, C. M. 2004, Ap&SS, 292, 619
Valenti, J. A., Marcy, G. W., & Basri, G. 1995, ApJ, 439, 939
Valenti, J. A., & Piskunov, N. 1996, A&AS, 118, 595
Vogt, S. S. 1978, PhD thesis, Texas Univ., Austin
Vogt, S. S., Penrod, G. D., & Hatzes, A. P. 1987, ApJ, 321, 496
Vogt, S. S., Tull, R. G., & Kelton, P. W. 1980, ApJ, 236, 308
Wade, G. A., Donati, J.-F., Landstreet, J. D., & Shorlin, S. L. S. 2000a, MNRAS, 313, 823
Wade, G. A., Donati, J.-F., Landstreet, J. D., & Shorlin, S. L. S. 2000b, MNRAS, 313, 851
Xiao, H. Y., Covey, K. R., Rebull, L., et al. 2012, ApJS, 202, 7
Yang, H., & Johns-Krull, C. M. 2011, ApJ, 729, 83
Yang, H., Johns-Krull, C. M., & Valenti, J. A. 2005, ApJ, 635, 466
Yang, H., Johns-Krull, C. M., & Valenti, J. A. 2007, ApJ, 133, 73
Yang, H., Johns-Krull, C. M., & Valenti, J. A. 2008, AJ, 136, 2286